AMERICAN SOCIETY FOR MICROBIOLOGY | Journal of Virology®

VIRUS-CELL INTERACTIONS

Axl Can Serve as Entry Factor for Lassa Virus Depending on the Functional Glycosylation of Dystroglycan

Chiara Fedeli,[a] Giulia Torriani,[a] Clara Galan-Navarro,[a,b] Marie-Laurence Moraz,[a] Hector Moreno,[a] Gisa Gerold,[c] Stefan Kunz[a]

[a]Institute of Microbiology, Lausanne University Hospital, Lausanne, Switzerland

[b]Laboratory of Lymphatic and Cancer Bioengineering, Institute of Bioengineering, École Polytechnique Féderale de Lausanne (EPFL), Lausanne, Switzerland

[c]TWINCORE, Center for Experimental and Clinical Infection Research, Institute for Experimental Virology, Hannover, Germany

ABSTRACT Fatal infection with the highly pathogenic Lassa virus (LASV) is characterized by extensive viral dissemination, indicating broad tissue tropism. The major cellular receptor for LASV is the highly conserved extracellular matrix receptor dystroglycan (DG). Binding of LASV depends on DG's tissue-specific posttranslational modification with the unusual O-linked polysaccharide matriglycan. Interestingly, functional glycosylation of DG does not always correlate with viral tropism observed *in vivo*. The broadly expressed phosphatidylserine (PS) receptors Axl and Tyro3 were recently identified as alternative LASV receptor candidates. However, their role in LASV entry is not entirely understood. Here, we examine LASV receptor candidates in primary human cells and found coexpression of Axl with differentially glycosylated DG. To study LASV receptor use in the context of productive arenavirus infection, we employed recombinant lymphocytic choriomeningitis virus expressing LASV glycoprotein (rLCMV-LASV GP) as a validated biosafety level 2 (BSL2) model. We confirm and extend previous work showing that Axl can contribute to LASV entry in the absence of functional DG using "apoptotic mimicry" in a way similar to that of other enveloped viruses. We further show that Axl-dependent LASV entry requires receptor activation and involves a pathway resembling macropinocytosis. Axl-mediated LASV entry is facilitated by heparan sulfate and critically depends on the late endosomal protein LAMP-1 as an intracellular entry factor. In endothelial cells expressing low levels of functional DG, both receptors are engaged by the virus and can contribute to productive entry. In sum, we characterize the role of Axl in LASV entry and provide a rationale for targeting Axl in antiviral therapy.

IMPORTANCE The highly pathogenic arenavirus Lassa virus (LASV) represents a serious public health problem in Africa. Although the principal LASV receptor, dystroglycan (DG), is ubiquitously expressed, virus binding critically depends on DG's posttranslational modification, which does not always correlate with tissue tropism. The broadly expressed phosphatidylserine receptor Axl was recently identified as an alternative LASV receptor candidate, but its role in LASV entry is unclear. Here, we investigate the exact role of Axl in LASV entry as a function of DG's posttranslational modification. We found that in the absence of functional DG, Axl can mediate LASV entry via apoptotic mimicry. Productive entry requires virus-induced receptor activation, involves macropinocytosis, and critically depends on LAMP-1. In endothelial cells that express low levels of glycosylated DG, both receptors can promote LASV entry. In sum, our study defines the roles of Axl in LASV entry and provides a rationale for targeting Axl in antiviral therapy.

KEYWORDS Axl, Lassa virus, attachment, dystroglycan, entry factor, macropinocytosis, receptor, viral entry

Received 12 September 2017 **Accepted** 4 December 2017

Accepted manuscript posted online 13 December 2017

Citation Fedeli C, Torriani G, Galan-Navarro C, Moraz M-L, Moreno H, Gerold G, Kunz S. 2018. Axl can serve as entry factor for Lassa virus depending on the functional glycosylation of dystroglycan. J Virol 92:e01613-17. https://doi.org/10.1128/JVI.01613-17.

Editor Terence S. Dermody, University of Pittsburgh School of Medicine

Address correspondence to Stefan Kunz, Stefan.Kunz@chuv.ch.

C.F. and G.T. contributed equally to this article.

The Old World arenavirus Lassa virus (LASV) is the causative agent of a severe viral hemorrhagic fever with high mortality in humans (1, 2) and is currently considered an important emerging pathogen by the World Health Organization (3). Carried in nature by persistent infection of reservoir rodent hosts of *Mastomys* species, LASV is endemic in large areas of Western Africa, where it causes several hundred thousand infections per year, with thousands of deaths. Transmission of LASV from rodents to humans occurs mainly via contaminated aerosolized rodent excreta and ingestion of contaminated food (1). Human-to-human transmission has been reported in nosocomial settings (4). Due to its transmissibility via aerosol (5) and high lethality, LASV is considered a category A agent by the Centers for Disease Control and Prevention (CDC) (6).

Following productive infection at the sites of entry, the virus enters the bloodstream and disseminates to lymph nodes, spleen, and liver. Severe LASV infection is characterized by extensive viral replication in many tissues, resulting in high viremia and progressive signs and symptoms of shock. Early targets of LASV during systemic dissemination are dendritic cells (DC) and macrophages, followed by infection of hepatocytes, endothelial cells, and epithelial cells of the lung and kidney (7). A highly predictive factor for disease outcome is the viral load, indicating a close competition between viral spread and replication and the patient's immune system (8). There is no licensed vaccine, and treatment is limited to supportive care and ribavirin, which reduces mortality when delivered early in infection (9). Drugs targeting early steps of the viral life cycle may delay viral spread, providing the immune system a window of opportunity to develop an antiviral immune response. An in-depth understanding of the molecular mechanisms underlying LASV cell entry into relevant target cells is therefore of great importance in developing novel and efficacious antiviral strategies.

Arenaviruses are enveloped negative-strand RNA viruses whose nonlytic life cycle is confined to the cytoplasm (10). The arenavirus genome is comprised of two RNA segments that code for two proteins each by an ambisense coding strategy. The small (S) RNA segment encodes the envelope glycoprotein precursor (GPC) and the nucleoprotein (NP), while the L segment encodes the matrix protein (Z) as well as the viral polymerase (L). GPC is synthesized as a single polypeptide and undergoes processing by signal peptidases and the proprotein convertase subtilisin kexin isozyme 1 (SKI-1)/site 1 protease (S1P), yielding an unusually stable signal peptide (SSP), N-terminal glycoprotein 1 (GP1), and transmembrane GP2. GP1 binds to cellular receptors, whereas GP2 mediates viral fusion and structurally resembles class I viral fusion proteins.

The interaction of a virus with its cellular receptor(s) is a key determinant for transmission, tissue tropism, and disease potential. The first cellular receptor for LASV and other Old World arenaviruses was identified as dystroglycan (DG), a ubiquitously expressed and highly conserved receptor for extracellular matrix (ECM) proteins (11). Dystroglycan is expressed in most developing and adult tissues, where it provides a molecular link between the ECM and the actin-based cytoskeleton. Initially encoded as a single polypeptide, DG is cleaved into the extracellular alpha-DG (α-DG) and membrane-anchored β-DG (12). In mammals, α-DG is subject to complex O-glycosylation, which is essential for its function as a receptor for ECM proteins and arenaviruses (13–15). During the biosynthesis of functional α-DG, the dually specific glycosyltransferase-like acetylglucosaminyltransferase (LARGE) attaches to the Xyl-α1-GlcA-3-β1-3 polysaccharide "matriglycan" (16, 17), which binds ECM proteins and arenaviruses (13, 18, 19). A genetic screen revealed that LASV closely mimics the molecular mechanisms of receptor recognition of ECM proteins (20). The recently solved high-resolution structure of LASV GP indicated that the trimeric virion spike engages DG-linked matriglycan polymers with high avidity (21).

The DG core protein is ubiquitously expressed in most mammalian cells and undergoes classical N- and mucin-type O-glycosylation. In contrast, the specific functional glycosylation of α-DG by LARGE is under tight tissue-specific control, making DG a "tunable" receptor (18) whose levels of virus-binding affinity greatly vary. Interestingly, functional glycosylation of DG in human and animal tissues does not always

correlate with susceptibility to LASV *in vivo* (7, 22, 23), suggesting the existence of alternative receptors. Using an expression cloning approach, the Tyro3/Axl/Mer (TAM) receptor tyrosine kinases Axl and Tyro3, as well as the C-type lectins DC-specific ICAM-3-grabbing nonintegrin (DC-SIGN) and LSECtin have been identified as candidate LASV receptors (24). Based on their restricted expression patterns, DC-SIGN and LSECtin may contribute to LASV entry into specific cell types, such as dendritic cells, but their exact role is currently unclear (25). The TAM kinases Axl and Tyro3 are conserved receptors for the phosphatidylserine (PS)-binding serum proteins Gas6 and protein S, which are involved in removal of apoptotic cells (26, 27). Over the past years, TAM kinases and other cellular PS receptors have been implicated in viral entry via "apoptotic mimicry," a mechanism initially described by Mercer and Helenius for poxviruses (28) that is characterized by recognition of PS displayed on the viral lipid envelope (29, 30). Viral apoptotic mimicry is increasingly recognized as an entry strategy for a broad spectrum of enveloped viruses and some nonenveloped viruses, including important emerging pathogens, such as Ebola, Dengue, West Nile, and Zika virus (29, 30). Currently, the exact role of TAM receptors in LASV entry is not entirely clear, and published data appear conflicting (24, 29, 31). The initial report identifying TAM kinases as candidate LASV receptors provided evidence of a role for Axl and Tyro3 in DG-independent entry of lentiviral LASV pseudotypes (24). However, a subsequent systematic study covering a large panel of emerging viruses, using different pseudotype platforms, concluded that Axl was unable to mediate productive LASV entry (31). Here, we sought to resolve these apparent contradictions and investigated the exact role of Axl in LASV entry in the context of productive arenavirus infection using a validated biosafety level 2 (BSL2) surrogate model. We further investigate the mechanism underlying Axl-mediated LASV entry and provide a rationale for targeting Axl in antiviral therapy.

RESULTS

Primary human cells coexpress Axl and differentially glycosylated DG. Histological examination of mammalian tissues revealed that DG's functional glycosylation by LARGE is under tight tissue-specific control, resulting in considerable variation in the lengths of DG-associated matriglycan chains (32), affecting DG's function as a LASV receptor. LARGE was originally discovered as a tumor suppressor gene (33), and its expression is frequently altered in immortalized tumor cell lines (34). In a first step, we therefore examined expression of functional DG and alternative LASV receptor candidates in a panel of primary human cells targeted by LASV *ex vivo*, including hepatocytes, endothelial cells, and epithelial cells (22). Primary human hepatocytes were isolated from liver specimens obtained after partial hepatectomy and cultured as described in Materials and Methods (35). As primary cell culture models for microvascular endothelial cells, human umbilical cord vascular endothelial cells (HUVEC) and human microvascular endothelial cells of the lung (HMVEC-L) were used. Primary human small-airway epithelial cells (SAEC) served as the model for primary respiratory epithelial cells. The extent of functional glycosylation of DG in these primary cells was assessed by Western blotting combining monoclonal antibody (MAb) IIH6, specific for the α-DG-linked matriglycan epitope, with MAb 8D5 directed to the β-DG core protein (36). As controls, we included the human fibrosarcoma line HT-1080, which is deficient in LARGE expression (24), and the human alveolar epithelial cell line A549, expressing functional DG (15). In line with *in vivo* data, primary hepatocytes expressed DG core protein without detectable matriglycan (32) (Fig. 1A). Both endothelial cell types expressed an underglycosylated α-DG form migrating at an apparent molecular mass of 100 to 110 kDa, whereas α-DG from SAEC migrated around 125 to 145 kDa, similar to the molecular mass of the form detected in A549 cells and in adult lung epithelia *in vivo* (37) (Fig. 1A). Examination of the expression of the candidate receptors Axl, Tyro3, and DC-SIGN revealed the presence of Axl in all cell types, whereas Tyro3 and DC-SIGN seemed absent. Together, the data indicated coexpression of Axl with differentially glycosylated DGs on primary human cells.

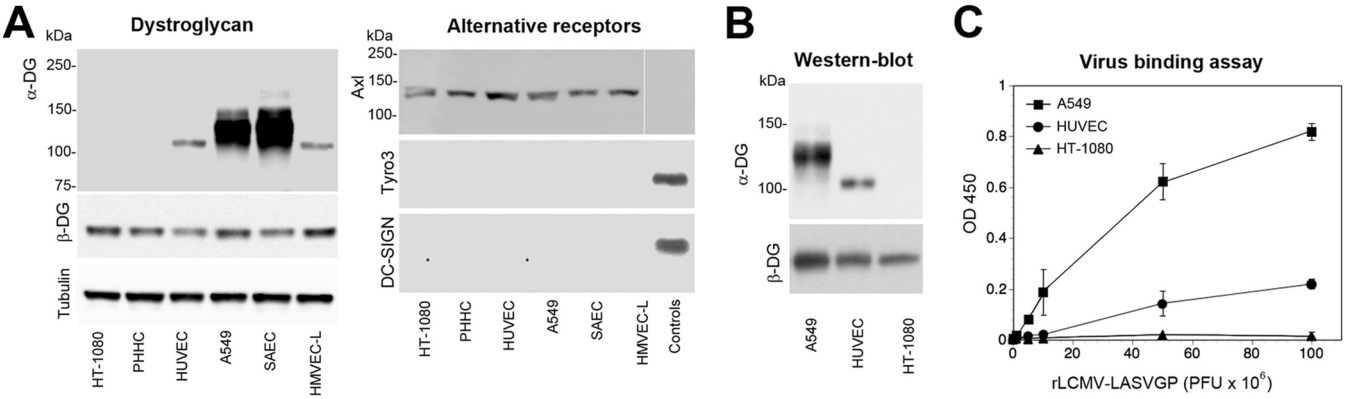

FIG 1 Primary human cells coexpress Axl and differentially glycosylated DG. (A) Detection of candidate LASV receptors in primary human cells. Total cell protein was extracted from primary human hepatocytes (PHHC), HUVEC, HMVEC-L, and SAEC, separated by SDS-PAGE, and blotted onto nitrocellulose. Functional DG was detected with MAb IIH6, which recognizes the matriglycan sugar polymers on α-DG. The presence of the core protein was probed with MAb 8D5 to β-DG, and α-tubulin was included as a loading control. A549 and HT-1080 cells were included as positive and negative controls, respectively. Axl, Tyro3, and DC-SIGN were detected with polyclonal Ab goat anti-human Axl, MAb 96201 anti-human Tyro3, and MAb 120507 anti-DC-SIGN. Human THP-1 monocytes and THP-1-derived immature dendritic cells were used as positive controls for Tyro3 and DC-SIGN, respectively (25). As a negative control for Axl, HEK293H cells were included. The negative-control lane of the Axl blot was taken from the same membrane and moved, as indicated by the thin white line. Primary antibodies were detected with HRP-conjugated secondary antibodies using enhanced chemiluminescence (ECL) for development. The observed differences in the apparent molecular masses of Axl in different cells were consistently observed and may be due to different glycosylation patterns. The expression levels of Axl in PHHC varied between donors, and a representative example was selected. (B) Western blot of WGA-purified DG. Dystroglycan was purified from the indicated cells by WGA affinity chromatography. Concentrated fractions were probed in a Western blot for functional glycosylation of α-DG with MAb IIH6 and for β-DG with MAb 8D5 as described for panel A. (C) Solid-phase virus binding assay. Equal amounts of DG purified from the indicated cells were immobilized in microtiter plates and incubated with the indicated concentrations of purified rLCMV-LASVGP. Bound virus was detected with MAb 83.6 to LASV GP2 using a biotinylated secondary antibody and HRP-conjugated streptavidin in a color reaction. Data are means $\pm$ standard deviations (SD) ($n = 3$).

Previous studies demonstrated that distinct apparent molecular masses of α-DG in SDS-PAGE are due to different lengths of the matriglycan chains (18, 36, 38). Recent structural data on the prefusion conformation of mature LASV GP suggest an avidity-based binding mode of the GP1 trimers to DG-linked matriglycan chains (21). To address this issue, we assessed virus binding affinity to differentially glycosylated DGs by employing a quantitative solid-phase binding assay (14). Since LASV is a BSL4 pathogen, work with live virus is restricted. We therefore used a recombinant lymphocytic choriomeningitis virus expressing the envelope GP of LASV strain Josiah (rLCMV-LASVGP). As viral entry is exclusively mediated by the viral envelope, this chimera represents a suitable BSL2 surrogate for study of LASV entry and has been widely used for the characterization of LASV cell tropism *in vitro* (39–42) and *in vivo* (43, 44). Dystroglycan was enriched from A549 cells, HUVEC, and HT-1080 cells by affinity purification using the lectin wheat germ agglutinin (WGA), which recognizes generic N-glycans (38) (Fig. 1B). Equal amounts of DG protein were immobilized in microtiter plates and incubated with increasing concentrations of purified virus. Bound virus was detected with MAb 83.6 to LASV GP2, as described previously (14). As shown in Fig. 1C, virus binding affinity indeed correlated with the apparent molecular mass of α-DG, consistent with the avidity-based binding mode proposed by the current structural model (21).

Axl can mediate productive LASV entry in the absence of functional DG. In line with histological evidence, our examination of LASV candidate receptor expression on primary human cells revealed that Axl can be coexpressed with DG that either lacks functional glycosylation or bears matriglycan chains of different lengths. Considering the conflicting reports in the literature (24, 31), we sought to clarify the exact contribution of Axl in LASV cell entry as a function of DG's posttranslational modification in the context of productive arenavirus infection, using our rLCMV-LASVGP chimera. A large body of evidence supports the current model of TAM receptor-mediated viral entry by apoptotic mimicry, involving recognition of PS in the virion envelope by the high-affinity ligands Gas6 and protein S (29), which are naturally present in serum (45, 46). The concentration of PS displayed in the viral envelope therefore influences virus

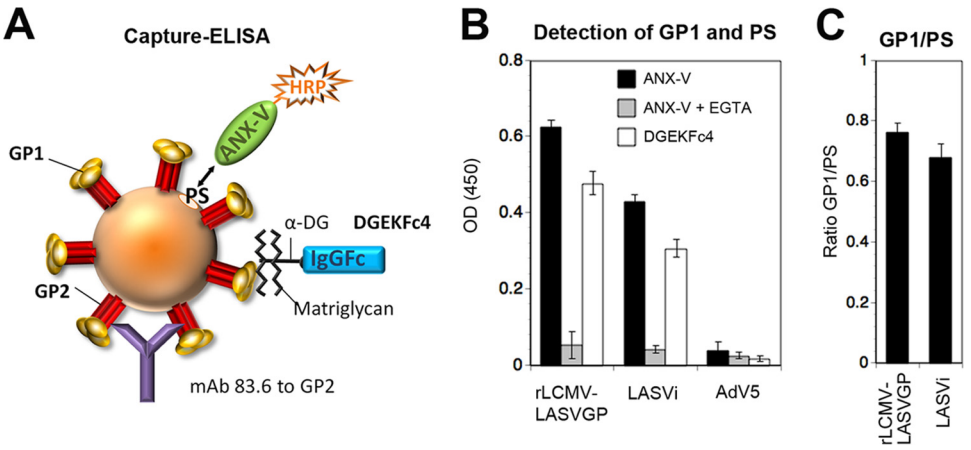

FIG 2 Determination of GP1/PS ratios in rLCMV-LASVGP and authentic LASV. (A) Schematic of the capture ELISA. Virus is captured by immobilized MAb 86.3, which recognizes a conserved nonneutralizing epitope in GP2. After removal of unbound material, bound virus is probed with ANX-V to detect PS, displayed in the lipid bilayer of the viral envelope, and DGEKFc4, which binds to GP1. For details, please see the text. (B) Detection of GP1 and PS. Purified rLCMV-LASVGP and authentic inactivated LASV were incubated with immobilized MAb 83.6, with the nonenveloped AdV5-GFP used as a negative control. After the plates were washed, bound virus was incubated with biotin-conjugated ANX-V in the presence and absence of EGTA, as well as DGEKFc4. Bound biotinylated ANX-V and DGEKFc4 were detected by streptavidin-HRP- and HRP-conjugated anti-human Fc antibody in a color reaction. Please note the reduced ANX-V binding in the presence of the Ca^{2+} chelator EGTA. Data are means ± SD ($n = 3$). (C) Ratios of GP1 to PS calculated for the virus preparations tested in panel B. OD (450), optical density at 450 nm; LASVi, inactivated LASV.

binding via Axl. Since functional DG is recognized by the viral envelope protein GP1, the exact ratio of LASV GP1 to PS in the viral envelope appears critical for studying receptor use. As a first step, we tried to validate our rLCMV-LASVGP chimera, comparing its GP1/PS ratio with that of authentic LASV using a capture enzyme-linked immunosorbent assay (ELISA) (Fig. 2A). To remove serum-derived PS-binding proteins that may interfere with our assay, viruses were treated with the Ca^{2+} chelator EGTA, which efficiently dissociates Gas6 and PS (45), followed by purification over a renografin gradient, as detailed in Materials and Methods. Purified virus was added to microtiter plates coated with MAb 83.6, which recognizes a highly conserved epitope in GP2 (47) and does not interfere with virus-receptor binding (11) (Fig. 2A). After specific capture of virus for 16 h in the cold, plates were washed and PS displayed on the viral envelope was detected with the PS-binding protein annexin V (ANX-V). LASV GP1 was detected using the recombinant virus-binding DG fragment DGEKFc4, which contains a C-terminal human IgG1 Fc moiety (48). Across different preparations, the GP1/PS ratios of rLCMV-LASVGP were similar to those of the authentic virus (Fig. 2B), validating our chimera as a suitable BSL2 model to investigate receptor use.

As our primary hepatocytes turned out to be challenging to manipulate *in vitro*, we needed a suitable cell model to study Axl-mediated cell entry of rLCMV-LASVGP in the absence of functional DG. After examination of a panel of cell lines, we opted for the fibrosarcoma cell line HT-1080, which lacks functional DG and expresses Axl, as do primary hepatocytes (Fig. 1A). To exclude any contribution of the remaining DG core protein, we depleted DG from HT-1080 cells using specific small hairpin RNAs (shRNAs) delivered by lentiviral vectors (Fig. 3A). Cells depleted of DG and controls were infected with rLCMV-LASVGP at a low multiplicity of infection (MOI) of 0.01. After 16 h, cells were fixed and productive infection was assessed by detection of LCMV NP using MAb 113 in an immunofluorescence assay (IFA). Depletion of DG core protein by >98% did not affect infection with rLCMV-LASVGP, excluding a significant contribution by it (Fig. 3B). In contrast, knockdown of Axl using validated small interfering RNAs (siRNAs) markedly reduced productive infection by rLCMV-LASVGP but not that by recombinant LCMV expressing the G protein of vesicular stomatitis virus (rLCMV-VSVG), which enters independently of TAM receptors (45) (Fig. 3C and D). The RNA interference (RNAi) data

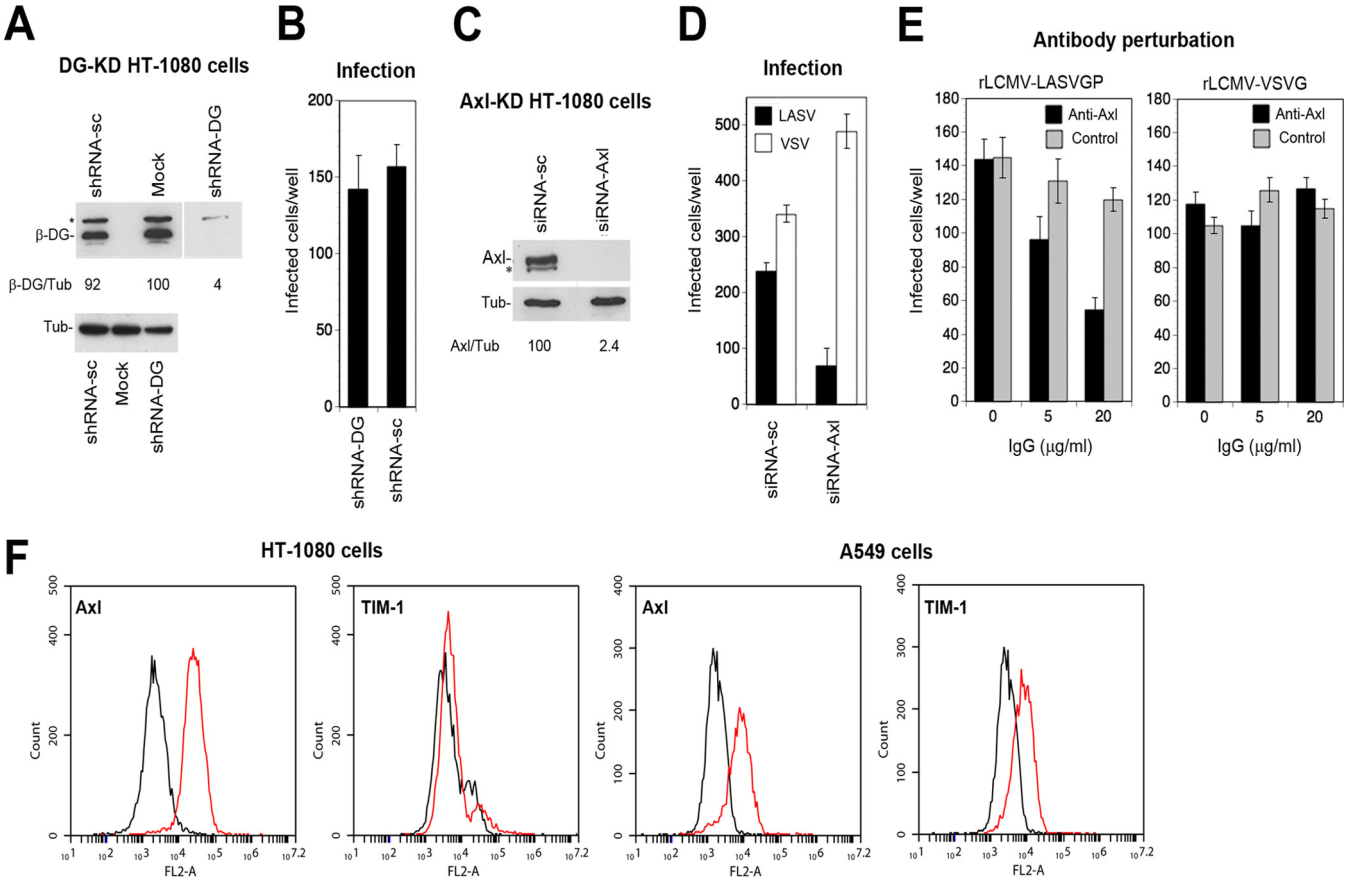

FIG 3 Axl can mediate productive LASV entry in the absence of functional DG. (A) Knockdown of DG in HT-1080 cells. HT-1080 cells either were transduced with a lentiviral vector expressing a DG-specific shRNA (shRNA-DG) or scrambled shRNA (shRNA-sc) or were mock transduced (mock), followed by selection with puromycin, as detailed in Materials and Methods. Depletion of DG core protein was verified in a Western blot using MAb 8D5 to β-DG and α-tubulin (Tub) as a loading control. The asterisk indicates an unspecific band. The lane corresponding to the sample of shRNA-DG-expressing cells was taken from the same membrane and moved, as indicated by the thin white line. Efficiency of depletion was assessed by densitometric analysis, followed by calculation of the signal ratios of β-DG/α-tubulin (β-DG/Tub). Numbers below the blot are percentages. (B) HT-1080 cells transduced with shRNA-DG or shRNA-sc (A) were seeded in 96-well plates and infected with rLCMV-LASVGP (300 PFU/well) for 1 h. Cells were washed with medium supplemented with 20 mM ammonium chloride to prevent secondary infection. After 16 h of incubation in the presence of ammonium chloride, cells were fixed and infection was detected by IFA using MAb 113 to LCMV NP combined with an Alexa 488-conjugated secondary antibody. Infection was quantified by counting the number of infected cells per well, with cell doublets considered single infection events. Data are means ± SD (n = 3). (C) Depletion of Axl from HT-1080 cells. HT-1080 cells were transfected with siRNAs to Axl (siRNA-Axl) and scrambled control siRNAs (siRNA-sc) as detailed in Materials and Methods. After 72 h, expression of Axl was detected in a Western blot using α-tubulin (Tub) as a loading control. In some blots, a lower-molecular-mass band (*) was detected. However, this was not consistently observed. Efficiency of Axl depletion was assessed by densitometry, followed by calculation of the signal ratios of Axl/α-tubulin (Axl/Tub). Numbers beneath the blot are percentages. (D) Infection of Axl-depleted HT-1080 cells. HT-1080 cells transfected with siRNA-Axl and siRNA-sc were infected with 300 PFU/well rLCMV-LASVGP (LASV) and rLCMV-VSVG (VSV), and infection was detected as described for panel B. Data are means ± SD (n = 3). (E) Blocking of Axl-mediated infection by antibody perturbation. HT-1080 cells were chilled on ice, washed with cold serum-free medium, and blocked with the polyclonal Ab goat anti-Axl (20 μg/ml) and control goat IgG for 2 h in the cold in the absence of serum. Cells were then incubated with 300 PFU/well of rLCMV-LASVGP (LASV) and 200 PFU/well of rLCMV-VSVG (VSV) in the presence of antibody for 2 h in the cold. Unbound virus was removed by washing and cells cultured in complete medium at 37°C. After 1 h, 20 mM ammonium chloride was added and infection detected as described for panel B. Data are means ± SD (n = 3). (F) Detection of Axl and TIM-1 on HT-1080 cells by flow cytometry. Live nonpermeabilized cells were stained with the indicated antibodies. Bound primary antibodies were detected by flow cytometry using a PE-conjugated secondary antibody. Black lines represent secondary antibody only, and red lines represent primary and secondary antibody. FL2-A, fluorescence intensity.

were confirmed by antibody (Ab) perturbation using a polyclonal Ab to Axl (Fig. 3E). Apart from TAM kinases, PS receptors of the T-cell immunoglobulin and mucin domain (TIM) family, in particular the broadly expressed TIM-1 protein, have been identified as candidate receptors for a range of enveloped viruses (29, 30, 49). We therefore examined the cell surface expression levels of Axl and TIM-1 on HT-1080 cells by flow cytometry. Our HT-1080 cells expressed robust levels of Axl but only negligible amounts of TIM-1 (Fig. 3F). In sum, our results confirm that endogenous levels of Axl in HT-1080 cells can contribute to LASV entry in the context of productive arenavirus infection in the absence of functional DG, in line with the results in the original report (24).

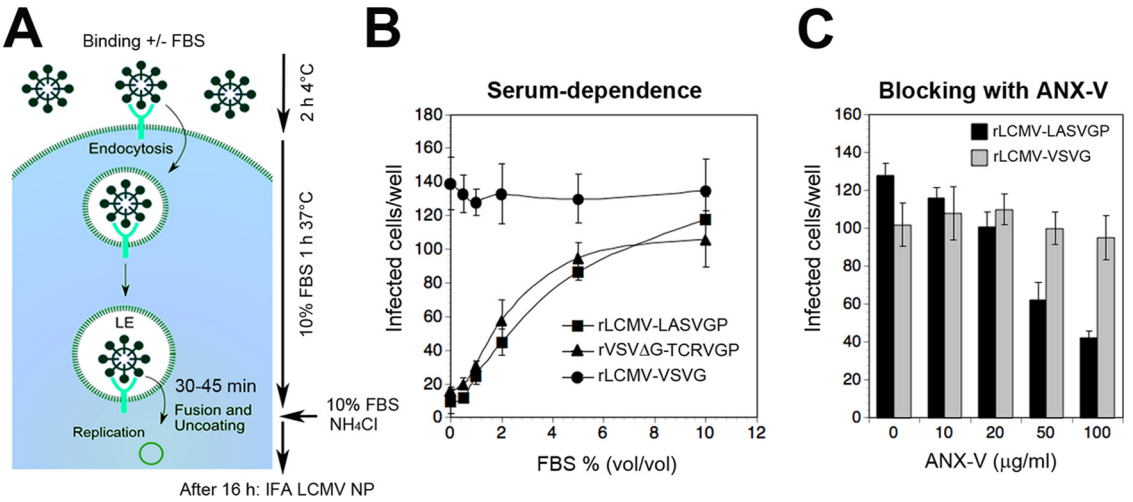

FIG 4 Axl-mediated LASV entry is serum dependent and requires the PS of the viral envelope. (A) Schema of the entry assay. For details, please see the text. LE, late endosome. (B) The entry of rLCMV-LASVGP into HT-1080 cells is serum dependent. Purified rLCMV-LASVGP (300 PFU/ml), rLCMV-VSVG (200 PFU/well), and rVSVΔG-TCRVGP (100 PFU/well) were pretreated with increasing concentrations of serum and added to HT-1080 cells cultured in 96-well plates for 2 h in the cold. Cells were washed 3 times and incubated with complete medium containing 10% (wt/vol) FBS at 37°C. After 1 h, complete medium containing 20 mM ammonium chloride was added, followed by 16 h of incubation in the presence of the lysosomotropic agent. Infection was detected by IFA as described for Fig. 3B. Data are means ± SD ($n = 3$). (C) Blocking of infection of HT-1080 cells with ANX-V. Purified rLCMV-LASVGP and rLCMV-VSVG were diluted in DMEM and pretreated with the indicated concentrations of ANX-V for 2 h in the cold. The virus–ANX-V mixture was then diluted 1:10 in complete medium containing 10% (wt/vol) FBS, resulting in a virus concentration of 300 PFU/well, and then added to HT-1080 cells for 1 h at 37°C. After 1 h, complete medium containing 20 mM ammonium chloride was added, followed by 16 h of incubation and detection of infection by IFA as described for Fig. 3B. Data are means ± SD ($n = 3$).

Axl-mediated LASV entry is serum dependent and requires PS of the viral envelope. A hallmark of Axl-mediated entry of most enveloped viruses via apoptotic mimicry is dependence on Gas6, which provides a molecular bridge between PS of the viral envelope and the TAM receptor (29, 45). In a first step, we assessed the serum dependence of Axl-mediated rLCMV-LASVGP attachment to HT-1080 cells. As a positive control, we used recombinant VSV pseudotypes bearing the envelope GP of the New World arenavirus Tacaribe virus (rVSVΔG-TCRVGP), which critically depend on PS receptors for cell entry (31). As a negative control, rLCMV-VSVG was included. Serum-starved HT-1080 cells were incubated with purified rLCMV-LASVGP, rVSVΔG-TCRVGP, and rLCMV-VSVG at a low multiplicity (MOI = 0.01) in the presence of increasing concentrations of serum in the cold to allow virus-cell attachment without internalization (Fig. 4A). After 2 h, unbound virus was removed, fresh complete medium containing serum was added, and cells were shifted to 37°C. After 1 h, the medium was supplemented with a 20 mM concentration of the lysosomotropic agent ammonium chloride. When added to cells, ammonium chloride raises the endosomal pH instantly and blocks low-pH-dependent endosomal escape of viruses, without causing overall cytotoxicity (50, 51). After 16 h, cells were fixed and productive infection was quantified by detection of LCMV NP in the IFA, whereas rVSVΔG-TCRVGP was detected via its green fluorescent protein (GFP) reporter. The presence of serum during viral attachment increased infection with rLCMV-LASVGP and rVSVΔG-TCRVGP in a dose-dependent manner but did not affect rLCMV-VSVG (Fig. 4B). In a complementary approach, we tried to mask PS displayed in the lipid bilayer of rLCMV-LASVGP with ANX-V. For this purpose, purified rLCMV-LASVGP and the rLCMV-VSVG control were pretreated with increasing concentrations of ANX-V, followed by infection of HT-1080 cells in the presence of serum. ANX-V blocked entry of rLCMV-LASVGP, but not of rLCMV-VSVG, in a dose-dependent manner, implicating PS in viral entry.

Kinetics of Axl-mediated viral endosomal escape. In productive infection, receptor-bound LASV is internalized by endocytosis, followed by delivery to late endosomes, where fusion occurs under low pH. In a next step to characterize Axl-

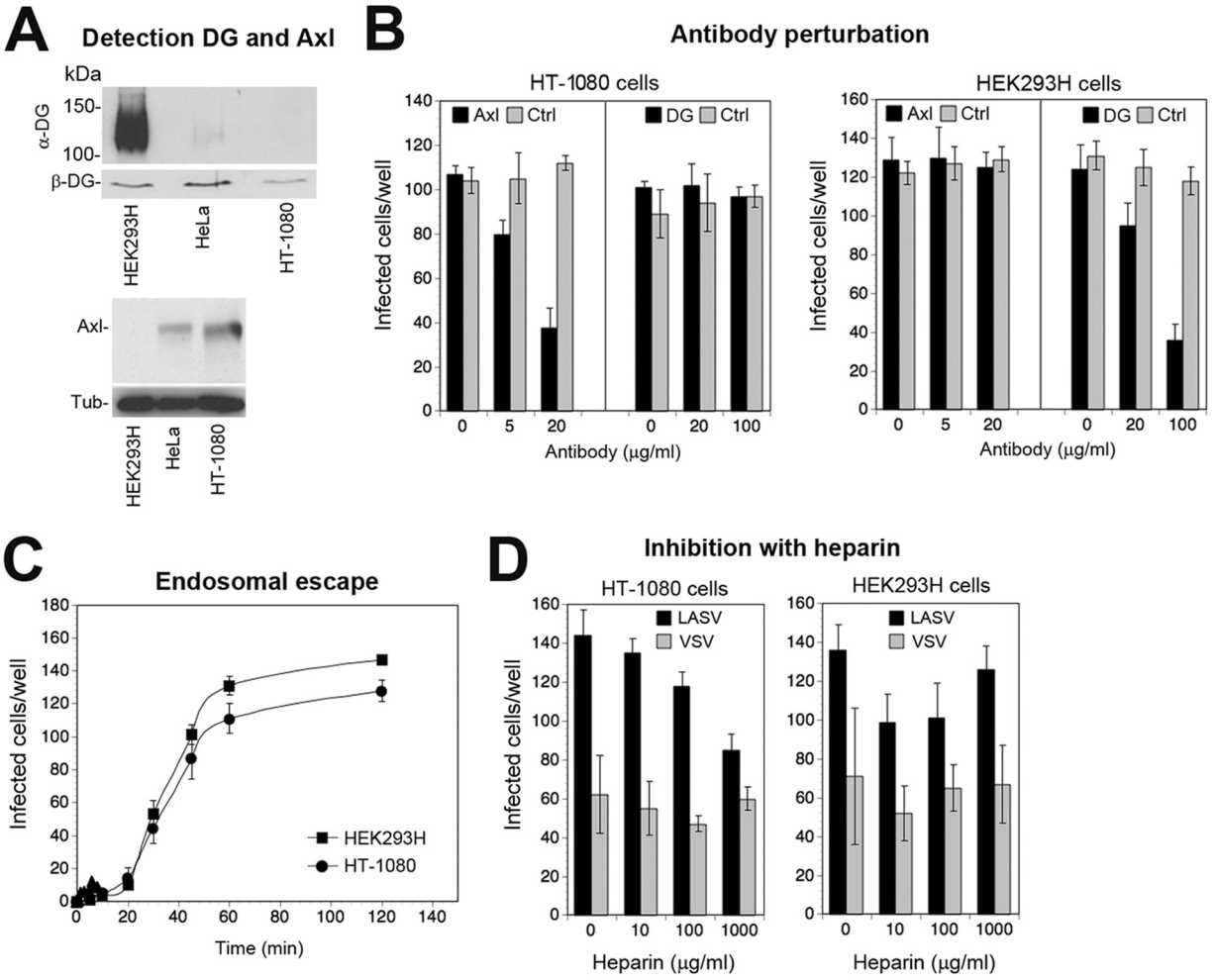

FIG 5 Kinetics of Axl-mediated viral endosomal escape. (A) Detection of functional DG and Axl in HEK293H and HT-1080 cells by Western blotting as described for Fig. 1A, including the LARGE-deficient cell line HeLa. Please note the residual signal for functionally glycosylated α-DG in HeLa cells, which was absent in HT-1080. (B) Verification of DG- and Axl-mediated entry of rLCMV-LASVGP into HT-1080 and HEK293H cells, respectively. The indicated cells were blocked with MAb IIH6 to glycosylated α-DG (100 μg/ml), polyclonal Ab goat anti-Axl (20 μg/ml), and control antibodies (Ctrl) for 2 h in the cold as described for Fig. 3E. Cells were then incubated with rLCMV-LASVGP at 100 PFU/well (HEK293H) and 300 PFU/well (HT-1080) for 2 h in the cold in the presence of antibodies. Cells were washed and kept in complete medium for 1 h at 37°C; then 20 mM ammonium chloride was added, the cells were cultured for 16 h and fixed, and infection was detected as described for Fig. 3B. Data are means ± SD (n = 3). (C) Endosomal escape of virus. rLCMV-LASVGP at 100 PFU/well (HEK293H) and 300 PFU/well (HT-1080) was attached to monolayers of the indicated cells in the cold for 2 h in complete medium. Unbound virus was removed, and cells were rapidly shifted to 37°C. At the indicated time points, 20 mM ammonium chloride was added and left throughout the experiment. After 16 h, infection was assessed by IFA as described for Fig. 3B. Given are means ± SD (n = 3). (D) Blocking of viral infection of HT-1080 and HEK293H cells with heparin. rLCMV-LASVGP (LASV) and rVSVΔG-VSVG (VSV) were diluted in complete medium and pretreated with the indicated concentrations of heparin for 1 h in the cold, followed by infection of cell monolayers for 1 h at 37°C in the presence of the inhibitor. After 1 h, complete medium containing 20 mM ammonium chloride was added, followed by 16 h of incubation and detection of infection by IFA as described for panel C. Data are means ± SD (n = 3).

mediated infection of rLCMV-LASVGP, we assessed the kinetics of viral endosomal escape. Specifically, we compared Axl-mediated entry of rLCMV-LASVGP into HT-1080 cells with that into HEK293H cells, which express highly glycosylated DG but lack Axl (Fig. 5A). Differential receptor use in HT-1080 cells (Axl) and HEK293H cells (DG) was verified by antibody perturbation (Fig. 5B). We compared the kinetics of late endosomal escape in HT-1080 and HEK293H cells, determining the time required by the virus from receptor attachment to become resistant to ammonium chloride. Virus was added to cells in the cold to allow receptor binding without internalization. The temperature was rapidly shifted to 37°C and ammonium chloride added at the time points indicated in Fig. 5 and left throughout the experiment. Readout of productive infection revealed similar half-times for endosomal escape of 30 to 45 min in the two cell types (Fig. 5C).

The data suggest that both Axl and DG can mediate endocytosis, followed by delivery to late endosomes with similar kinetics.

Heparan sulfate proteoglycans contribute to LASV entry via Axl but not via DG. A recent haploid screen for LASV entry factors in DG null cells uncovered several genes involved in the biosynthesis of heparan sulfate as candidates, suggesting a role for glycosaminoglycans in DG-independent LASV entry (52). To address this issue experimentally in the context of Axl-mediated cell entry, we preincubated rLCMV-LASVGP and rVSVΔG-VSVG with increasing concentrations of heparin in the cold. Subsequent infection of HT-1080 cells revealed an incremental, but consistent, dose-dependent reduction of Axl-mediated rLCMV-LASVGP (Fig. 5D). In contrast, infection of HEK293H cells via DG seemed unaffected by heparin (Fig. 5D). The data support the genetic studies (52) and suggest a contribution of heparan sulfate in DG-independent LASV cell entry in our system.

Virus-induced Axl tyrosine kinase activation is required for rLCMV-LASVGP entry. Engagement of cellular receptors by viruses frequently induces cellular signaling that can serve as a "knock on the door" to prime the host cell for further steps of infection (53–55). In previous studies, recombinant full-length Axl overexpressed in otherwise-refractory cell lines enhanced entry of LASV pseudotypes (24). Deletion of the cytosolic tyrosine kinase domain or insertion of "kinase-dead" mutations reduced LASV pseudotype infection, providing first evidence of a role for Axl signaling in LASV entry (24). To confirm these findings with endogenous Axl in the context of productive arenavirus infection, we used the novel small-molecule Axl tyrosine kinase inhibitor R428, which shows high selectivity and fast drug action (56, 57). To minimize the duration of drug exposure and unwanted off-target effects, we performed a drug washout assay, outlined in Fig. 6A. Briefly, HT-1080 cells were pretreated for 30 min with the inhibitor, followed by infection with rLCMV-LASVGP at a low multiplicity (MOI = 0.01) in the presence of drug. As positive and negative controls, we included rVSVΔG-TCRVGP and nonenveloped adenovirus 5 (AdV5)-GFP, respectively. After 1 h, the drug was washed out using medium containing ammonium chloride to block further entry. Productive infection was detected after 16 h by IFA. The Axl inhibitor R428 reduced rLCMV-LASVGP and rVSVΔG-TCRVGP infection in a dose-dependent manner, whereas AdV5-GFP was not affected (Fig. 6B and C). To validate cell entry as the main target of R428, we performed "time-of-addition" experiments. As shown in Fig. 6D, the Axl inhibitor was highly active against rLCMV-LASVGP when added before or during infection but had only a mild effect at later time points postentry. The nucleoside analogue ribavirin, which inhibits replication of the viral core, was active at all time points during infection, as expected (Fig. 6D).

The observed inhibition of Axl-mediated entry by R428 confirmed that Axl tyrosine kinase activity was indeed required for rLCMV-LASVGP entry, in line with the original report (24). Next, we addressed whether engagement of cellular Axl by the virus could activate receptor signaling or whether Axl tyrosine kinase activity served merely as a permissive signal. To this end, we preincubated purified rLCMV-LASVGP with 10% fetal bovine serum (FBS), followed by ultracentrifugation through a sucrose cushion. Pelleted virus was washed and resuspended in Hanks' balanced salt solution (HBSS), and infectious titers were verified by IFA. As a control, we included a mock preparation produced from the supernatants of uninfected cells by the same procedure, as described in Materials and Methods. Serum-starved HT-1080 cells were incubated with rLCMV-LASVGP at a high multiplicity of infection (50 PFU/cell) and equivalent amounts of a mock preparation in the cold to prevent membrane trafficking and signaling. After removal of unbound virus, cells were rapidly shifted to 37°C and lysed at the time points indicated in Fig. 6. Total Axl was immunoprecipitated (IP) with polyclonal anti-Axl antibody. Receptor autophosphorylation was detected by Western blotting using a MAb to tyrosine phosphate, as described previously (58). As shown in Fig. 6E, engagement of rLCMV-LASVGP induced detectable Axl tyrosine phosphorylation above background within circa 10 min. In sum, the data suggest that virus-induced Axl tyrosine kinase activity is required for DG-independent rLCMV-LASVGP entry.

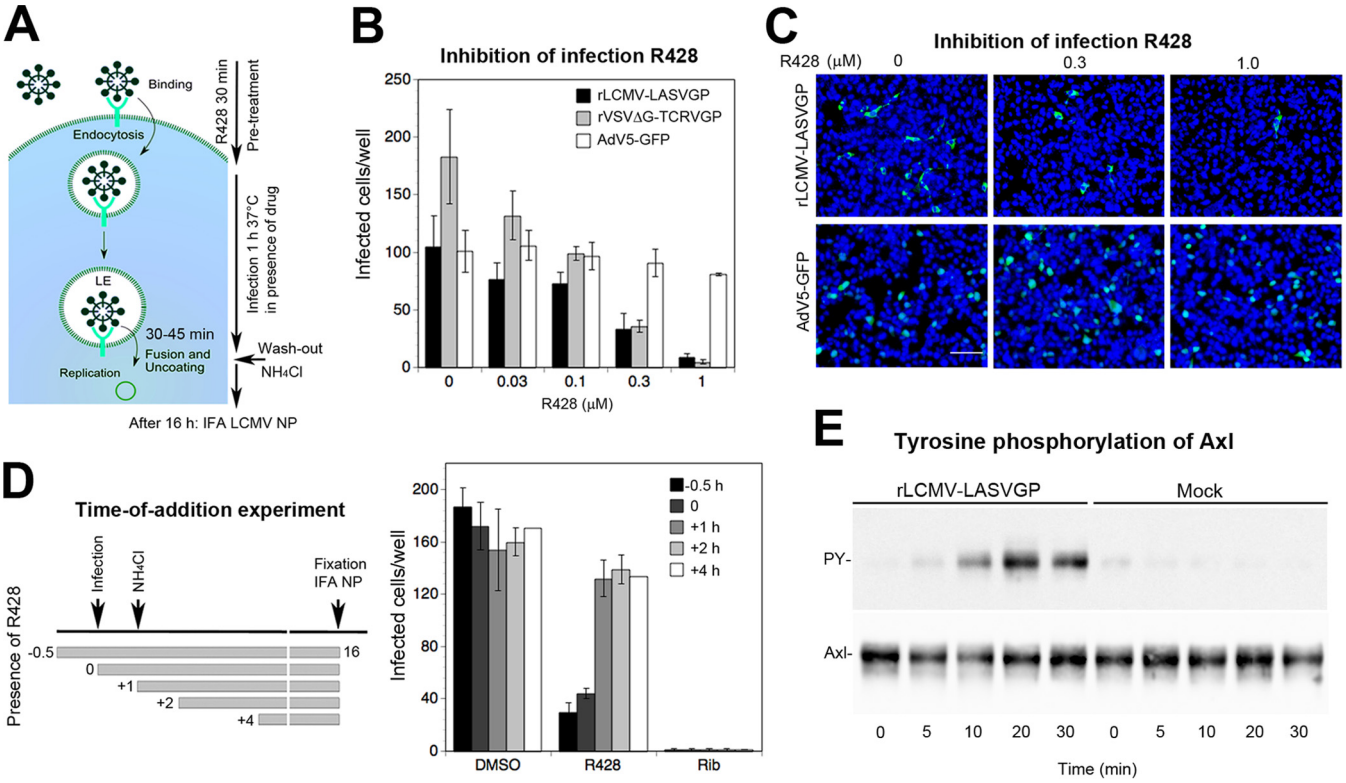

FIG 6 Virus-induced Axl tyrosine kinase activity is required for rLCMV-LASVGP entry. (A) Schema of the inhibitor washout experiment. For details, please see the text. LE, late endosome. (B) Infection of rLCMV-LASVGP depends on the activity of the Axl tyrosine kinase. HT-1080 cells were pretreated with the Axl tyrosine kinase inhibitor R428 at increasing concentrations for 30 min, followed by infection with the indicated viruses at 200 PFU/well in the presence of drug. After 1 h, cells were washed 3 times with medium containing 20 mM ammonium chloride, followed by 16 h of incubation in the presence of the lysosomotropic agent. Infection was detected by IFA as described for Fig. 3B. Data are means ± SD ($n = 3$). (C) Example of the inhibition of rLCMV-LASVGP infection by R428 revealed by IFA using MAb 113 to LCMV NP (green) and counterstaining of nuclei (DAPI; blue). Note the similar intensities of NP staining with increasing inhibitor concentrations (bar = 50 μm). The lower panel shows AdV5-GFP used as a negative control. NP- or GFP-positive cells were scored, with cell doublets considered single infectious events. (D) Time-of-addition experiment. HT-1080 cells were infected with rLCMV-LASVGP (300 PFU/well), with R428 or ribavirin (Rib) added at the different time points pre- or postinfection at 0.5 μM or 100 μM, respectively. Virus was added at time point 0, followed by washing and addition of ammonium chloride after 1 h. Ammonium chloride was kept throughout the experiment, and cells were subjected to IFA after 16 h. Data are means ± SD ($n = 3$). Examination of cell viability by the CellTiter-Glo assay reveled no significant toxicity of R428 under our experimental conditions (data not shown). (E) Engagement of rLCMV-LASVGP induces activation of Axl tyrosine kinase. Serum-starved HT-1080 cells were incubated with rLCMV-LASVGP at 50 PFU/cell and equivalent amounts of mock preparation for 2 h in the cold. Unbound virus was removed, and cells were shifted to 37°C. At the indicated time points, cells were lysed and Axl was isolated by IP with polyclonal Ab goat anti-Axl immobilized on a Sepharose matrix. Immunocomplexes were eluted, followed by SDS-PAGE using 5.5% (wt/vol) running gels. Total Axl protein in IP was revealed in a Western blot using a mouse MAb, anti-Axl (10% of sample), and tyrosine phosphorylation was detected by an MAb to tyrosine phosphate (90% of sample). For detection, TrueBlot HRP-conjugated anti-mouse IgG was used in ECL assays. Blots for tyrosine phosphate (PY) were exposed for 2 min and blots detecting total Axl for 10 s.

Axl-dependent LASV cell entry involves macropinocytosis and requires LAMP-1. Although TAM receptors have been implicated in viral entry via apoptotic mimicry for many viruses (29), the endocytotic pathway(s) underling TAM-mediated virus uptake remains largely unknown. Early studies on Ebola virus demonstrated that engagement of Axl by the virus can enhance macropinocytosis (59). However, more-recent work on Zika virus provided evidence for clathrin-mediated endocytosis (CME) (58), suggesting important virus-specific differences. To characterize the Axl-dependent entry pathway used by rLCMV-LASVGP in HT-1080 cells, we employed a panel of well-described diagnostic inhibitors of known cellular factors implicated in CME and macropinocytosis (60, 61) (Table 1).

To assess the clathrin and dynamin dependence of rLCMV-LASVGP entry via Axl, we used the inhibitor pitstop-2, which prevents ligand binding to the N-terminal domain of clathrin, and the dynamin inhibitors Dynasore and Dyngo 4a. To target preferentially viral entry and minimize off-target effects, inhibitors were tested in the entry assay outlined in Fig. 6A. As a positive control, a recombinant VSV expressing GFP (rVSV-GFP) was used. Pitstop-2, Dynasore, and Dyngo 4a only mildly affected rLCMV-LASVGP but

TABLE 1 Panel of diagnostic inhibitors used in the study

Inhibitor	Target	Concns (μM)
Dynasore	Dynamin	40, 80
Dyngo 4a	Dynamin	10, 20
Pitstop-2	Clathrin	2, 8
EIPA	NHE	10, 20, 40
Cytochalasin D	Actin	5, 10
Latrunculin A	Actin	0.5, 1
Jasplakinolide	Actin	0.5, 1
Pirl1	Cdc42	5, 10
NSC237766	Rac1	10, 25
CT04	RhoA	2, 5
IPA-3	PAK1	20, 40
ML7	Myosin light-chain kinase	20, 80
Blebbistatin	Myosin kinase II	10, 20

reduced infection with rVSV-GFP (62) (Fig. 7A). In a complementary approach, the clathrin heavy chain was depleted by RNAi (39). Knockdown of >95% of the clathrin heavy chain (Fig. 7B) did not affect rLCMV-LASVGP entry (Fig. 7C), supporting the possibility of a clathrin-independent pathway.

A conserved hallmark of viral entry via macropinocytosis is dependence on sodium proton exchangers (NHE) that are sensitive to amiloride drugs (60). Inhibition with 5-(*N*-ethyl-*N*-isopropyl) amiloride (EIPA) reduced rLCMV-LASVGP entry in a dose-dependent manner but only mildly affected rLCMV-VSVG entry (Fig. 7D). A second conserved feature of macropinocytosis is actin dependence (53, 63). To address this issue, cells were treated with the inhibitors cytochalasin D and latrunculin A, which disrupt actin filaments, as well as jasplakinolide, a drug that stabilizes actin fibers and blocks actin dynamics. Pretreatment with all actin inhibitors markedly reduced infection with rLCMV-LASVGP without affecting overall cell viability (Fig. 7E). The small GTPases Cdc42, Rac1, and RhoA represent important downstream effectors of NHE involved in actin regulation (64). Using the well-characterized inhibitors Pirl1, NSC23766, and CT04, we addressed the role of Cdc42, Rac1, and RhoA in Axl-mediated LASV entry. Pirl1 and NSC23766, but not CT04, specifically reduced productive infection with rLCMV-LASVGP, pinpointing Cdc42 and Rac1, but not RhoA, as entry factors (Fig. 7F). The differential roles of Cdc42, Rac1, and RhoA in viral entry versus the classical macropinocytosis observed here resemble those of other viral systems, e.g., respiratory syncytial virus (61). Infection of rLCMV-LASVGP was likewise reduced after inhibition of the Cdc42 downstream effector p21-activating kinase 1 (PAK-1) with IPA-3 (Fig. 7G). Productive entry of viruses via macropinocytosis frequently depends on non-muscle myosin II, required for membrane fission during the formation of early macropinosomes (63). To address this issue, HT-1080 cells were treated with blebbistatin, an inhibitor of myosin II as well as the myosin light-chain kinase inhibitor ML-7. As shown in Fig. 7G, both inhibitors specifically reduced the entry of rLCMV-LASVGP, suggesting that Axl-mediated entry of rLCMV-LASVGP involves a pathway related to macropinocytosis.

Upon entry via DG, LASV is rapidly delivered to the late endosome, where the virus undergoes a receptor switch and engages the late endosomal/lysosomal resident protein LAMP-1, which is essential for efficient fusion (52, 65, 66). Although most Old World arenaviruses can use DG as a receptor, the ability to hijack LAMP-1 as a late endosomal entry factor is unique to LASV (67). We therefore investigated whether LAMP-1 was also needed for Axl-mediated LASV entry into HT-1080 cells. Depletion of LAMP-1 by specific siRNAs impaired rLCMV-LASVGP entry into HT-1080 cells, suggesting an essential role for LAMP-1 as a late endosomal entry factor also for Axl-mediated entry (Fig. 7H and I).

Axl can contribute to LASV entry into endothelial cells. Endothelial cells represent important targets for LASV late in infection, and functional perturbation of the vascular endothelium precedes shock and death in cases of fatal Lassa fever (68). Early studies revealed that microvascular endothelial cells are highly susceptible to LASV

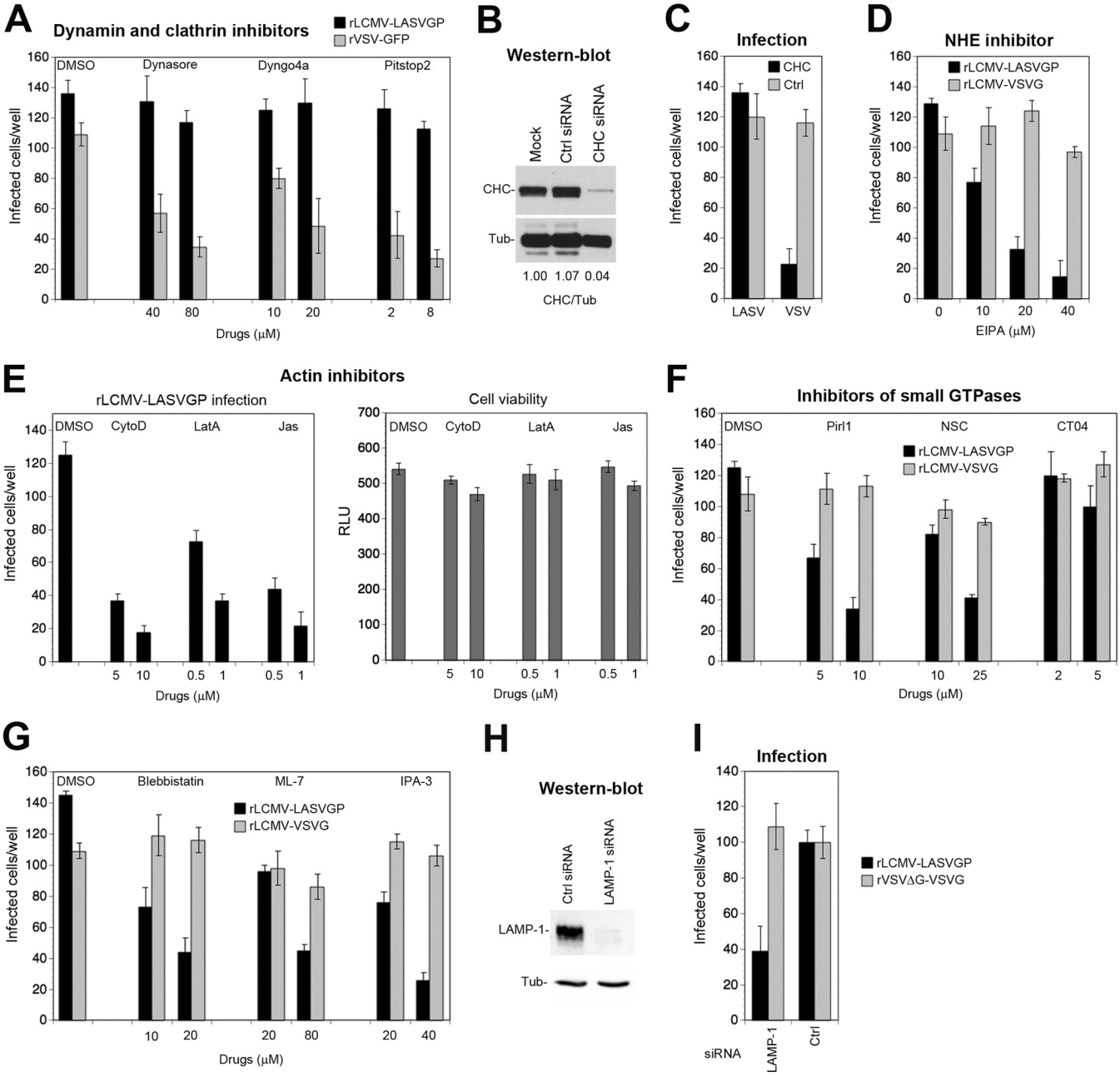

FIG 7 Axl-dependent LASV cell entry involves macropinocytosis and requires LAMP-1. (A) Axl-mediated entry of rLCMV-LASVGP is independent of dynamin and clathrin. HT-1080 cells were pretreated with inhibitors for dynamin-2 (Dynasore, Dyngo 4a) and clathrin (pitstop-2) at the indicated concentrations for 30 min, followed by infection with rLCMV-LASVGP (300 PFU/well) and rVSV-GFP (100 PFU/well) in complete medium in the presence of drugs. After 1 h, cells were washed 3 times with medium containing 20 mM ammonium chloride, followed by incubation in the presence of the agent. After 16 h, the cells were fixed, and infection was detected by IFA using MAb 113 to LCMV NP as described for Fig. 3B. Infection with rVSV-GFP was assessed after 8 h by detection of the enhanced-GFP reporter by direct-fluorescence microscopy. (B) Depletion of the clathrin heavy chain (CHC) by RNAi. HT-1080 cells were either transfected with a pool of siRNAs specific for the clathrin heavy chain or control scrambled siRNAs or mock transfected as described for Fig. 3C. After 72 h, expression of the clathrin heavy chain was detected in a Western blot using α-tubulin (Tub) as a loading control. The efficiency of clathrin heavy-chain depletion was assessed by densitometry, followed by calculation of the signal ratios of the clathrin heavy chain/α-tubulin (CHC/Tub). (C) HT-1080 cells subjected to RNAi were infected with rLCMV-LASVGP (LASV) at 300 PFU/well and rLCMV-VSVG (VSV) at 100 PFU/well for 1 h. Infection was detected by IFA as described for panel A. Data represent means $\pm$ SD ($n = 3$). (D) The amiloride drug EIPA blocks Axl-mediated entry of rLCMV-LASVGP. HT-1080 cells were pretreated with the indicated concentrations of EIPA for 30 min, followed by infection with rLCMV-LASVGP (300 PFU/well) and rLCMV-VSVG (100 PFU/well) in the presence of drugs for 1 h, and infection was detected by IFA as described for panel A. (E) Actin inhibitors block Axl-dependent rLCMV-LASVGP infection without causing cell toxicity. HT-1080 cells were pretreated with the indicated concentrations of cytochalasin D (CytoD), latrunculin A (LatA), and jasplakinolide (Jas) for 30 min, followed by infection with rLCMV-LASVGP (300 PFU/well) as described for panel A. Data are means $\pm$ SD ($n = 3$). Cell viability was monitored by the CellTiter-Glo assay as described in Materials and Methods by measuring cellular ATP levels in a luminescence assay. Data are displayed in relative light units (RLU) and are means $\pm$ SD ($n = 3$). (F) Axl-mediated entry of rLCMV-LASVGP depends on Cdc42 and Rac1 but not RhoA. HT-1080 cells were pretreated with a DMSO vehicle control or the inhibitors Pirl1 (Cdc42), NSC23766 (Rac1), and CT04 (RhoA) at the indicated concentrations, followed by infection with rLCMV-LASVGP (300 PFU/well) and rLCMV-VSVG (100 PFU/well) for 1 h in the presence of drugs, and infection was detected as described for panel A. Values are means $\pm$ SD ($n = 3$). (G) Axl-dependent

(Continued on next page)

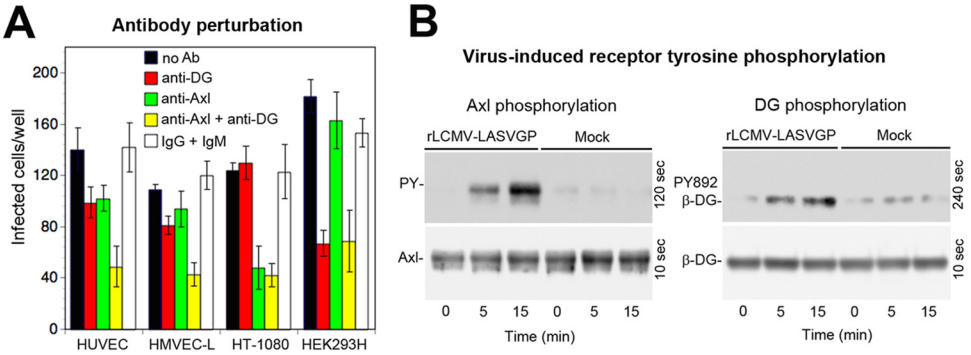

FIG 8 Axl contributes to LASV entry into endothelial cells. (A) Antibody perturbation of rLCMV-LASVGP entry in microvascular endothelial cells. Confluent monolayers of HUVEC and HMVEC-L were blocked with MAb IIH6 to glycosylated α-DG (anti-DG; 100 μg/ml), polyclonal Ab goat anti-Axl (anti-Axl; 20 μg/ml), the combination of both antibodies (anti-DG + anti-Axl), a combination of control antibodies (IgG + IgM), and medium only (no Ab) in the absence of serum for 2 h in the cold as described for Fig. 5B. HT-1080 cells and HEK293H cells were included as positive controls for Axl- and DG-mediated viral entry, respectively. Cells were then incubated with rLCMV-LASVGP at 300 PFU/well (HUVEC and HMVEC-L), 100 PFU/well (HEK293H), and 300 PFU/well (HT-1080) for 2 h in the cold in the presence of antibodies. Cells were washed and incubated with complete medium. After 16 h of incubation in the presence of ammonium chloride, cells were fixed and infection was detected as described for Fig. 3B. Data are means $\pm$ SD ($n = 3$). (B) Entry of rLCMV-LASVGP into HMVEC-L induces tyrosine phosphorylation of Axl and DG. Monolayers of HMVEC-L were incubated with rLCMV-LASVGP (50 PFU/cell) and equivalent amounts of a mock preparation for 2 h in the cold. Unbound virus was removed, and cells were shifted to 37°C. At the indicated time points, cells were lysed. Total protein was extracted from 10% of the cleared lysate and probed in a Western blot with MAb cl14a (anti-β-DG PY892) and antibody 8D5 to β-DG. The positions of β-DG and β-DG PY892 are indicated. Blots for β-DG PY892 were exposed for 4 min, and blots detecting total β-DG were exposed for 10 s. Axl was isolated by IP from 90% of the lysate, and tyrosine phosphorylation of Axl was detected as described for Fig. 6E. Blots for tyrosine phosphate (PY; 90% of the sample) were exposed for 2 min, and blots detecting total Axl (10% of the sample) were exposed for 10 s.

infection *in vitro* and can become prodigious sources of infectious virus (69). Examination of LASV candidate receptor expression in HUVEC and HMVEC-L in our present study revealed coexpression of Axl with an underglycosylated form of DG, showing relatively low virus binding affinity (Fig. 1). To address the relative contributions of DG and Axl to LASV entry, HUVEC and HMVEC-L were blocked with antibodies specific to Axl and functional DG, either alone or in combination, followed by infection. Perturbation of individual receptors hardly affected rLCMV-LASVGP entry, whereas the antibody combination lowered infection significantly (Fig. 8A), suggesting that both Axl and DG may contribute to infection.

Previous studies with human epithelial cells revealed that engagement of cellular DG by LASV GP induces tyrosine phosphorylation of β-DG's cytosolic domain, resulting in dissociation from the cytoskeletal adaptor protein utrophin, which may facilitate internalization of the virus-receptor complex (41). In a next step, we therefore assessed virus-induced tyrosine phosphorylation of Axl and DG in endothelial cells. Monolayers of HMVEC-L were exposed to rLCMV-LASVGP and to a mock preparation. After removal of unbound virus, cells were rapidly shifted to 37°C and lysed at the time points indicated in Fig. 8. Activation of Axl was detected as described above (Fig. 6E). Virus-induced tyrosine phosphorylation of DG was examined in a Western blot using a MAb that specifically recognizes β-DG phosphorylated at residue Y892, located in a C-terminal PPPY motif implicated in utrophin binding (41, 70). In HMVEC-L, entry of rLCMV-LASVGP induced tyrosine phosphorylation of Axl and DG with similar kinetics, suggesting that both receptors were engaged (Fig. 8B).

FIG 7 Legend (Continued)
entry of rLCMV-LASVGP requires PAK1, non-muscle myosin II, and myosin light-chain kinase. HT-1080 cells were treated with the indicated concentrations of IPA-3, blebbistatin, and ML-7, followed by infection with rLCMV-LASVGP (300 PFU/well) and rLCMV-VSVG (100 PFU/well) as described for panel D. Data are means $\pm$ SD ($n = 3$). (H) Knockdown of LAMP-1 by RNAi. HT-1080 cells were transfected with siRNAs specific for LAMP-1 and control scrambled siRNAs. After 48 h, depletion of LAMP-1 was verified in a Western blot using α-tubulin (Tub) as a loading control. (I) Axl-dependent infection of rLCMV-LASVGP depends on LAMP-1. LAMP-1-depleted and control HT-1080 cells were infected with rLCMV-LASVGP at 300 PFU/well and rVSVΔG-VSVG (100 PFU/well) for 1 h. Infection was detected by IFA as described for panel A. Data are means $\pm$ SEM ($n = 3$ for rLCMV-LASVGP and $n = 2$ for rVSVΔG-VSVG).

DISCUSSION

Many important human-pathogenic viruses evolved to use different receptors. However, the exact operational definitions of a receptor, coreceptor, and attachment and entry factor are frequently not straightforward and critically depend on species and cell type (55, 71). For LASV, the situation seems particularly complicated, considering the remarkably complex tissue-specific posttranslational modification of its major receptor, DG, which results in a large spectrum of receptor variants with strikingly different virus-binding affinities (72). The specific function of DG as a LASV receptor in a particular cell type appears therefore as a complex function of the expression of >20 genes currently implicated in the biosynthesis of functional DG (13). As for many other emerging enveloped viruses, the broadly specific cellular PS receptors Axl and Tyro3 have been proposed as candidate LASV receptors (29, 30). However, the published data on their specific role in LASV appear conflicting (24, 31). In the present study, we thought to clarify and characterize the roles of Axl in LASV entry.

The functional glycosylation of DG and expression of TAM receptors are frequently altered in tumor cells (34, 73). In a first step of our study, we therefore examined the expression of LASV candidate receptors in relevant primary human cell types cultured *ex vivo*. In primary human hepatocytes derived from liver biopsy specimens, we could not detect functional DG, in line with histological findings for adult liver tissue (23). The detection of Axl in our primary liver cells was further consistent with the recently reported Axl expression in healthy human hepatic tissue (74). Endothelial and epithelial cells are highly sensitive to LASV infection *in vitro* and *in vivo* (69, 75) and represent important targets for the virus late in disease (1, 7). Our examination of LASV candidate receptors in primary microvascular endothelial cells and respiratory epithelial cells revealed differential glycosylation of DG, which correlated with distinct virus binding affinities, emphasizing the current concept of DG as a tunable receptor (13, 18). Both endothelial and epithelial cells expressed Axl, in line with recent reports (76, 77). In sum, our results obtained from primary human cells are consistent with existing histological and biochemical *in vivo* data and confirm the idea that susceptible human cell types coexpress Axl with differentially glycosylated DG.

The susceptibility of a given cell type to LASV at the level of entry is likely a complex function of DG glycosylation and the expression levels of alternative receptors like Axl. The specific contributions of DG and Axl to LASV attachment and entry further critically depend on the exact GP1/PS ratio in the virion particles. Using a capture ELISA, we consistently found GP1/PS ratios in the envelopes of rLCMV-LASVGP that were comparable to those of authentic LASV, validating our chimera as a suitable BSL2 model for entry studies in the context of productive arenavirus infection.

In a first step, we confirmed the findings of the original report by Shimojima and colleagues (24) showing that Axl can indeed contribute to LASV entry in the context of productive arenavirus infection in the absence of functional DG. We then characterized Axl-mediated virus-cell attachment and found similarities to the model of apoptotic mimicry proposed for many viruses (29, 30). Using our rLCMV-LASVGP chimera, we further provide the first experimental evidence that heparan sulfate can facilitate DG-independent LASV entry via Axl, in line with a recent genetic screen (52).

Axl-mediated entry of several viruses requires receptor signaling through the receptor's cytosolic tyrosine kinase domain (58, 77–79). Interestingly, in most cases studied so far, including those of the flaviviruses Dengue, West Nile, and Zika virus, Axl signaling seems to not be required for virus internalization but promotes later steps of viral multiplication, increasing infectious virus production (58, 77, 78). In addition to having a role in removing apoptotic cells, TAM receptors play a crucial role in the negative regulation of innate immune signaling by regulating the host cell's type I interferon (IFN-I) response (27, 80, 81). In a current model, engagement of Axl by enveloped viruses downregulates innate immune signaling, blunting the IFN-I response and thus promoting viral replication (29, 30, 78). As with Zika virus (58), we found that engagement of cellular Axl by rLCMV-LASVGP induces rapid receptor phosphorylation.

However, a combination of drug washout and time-of-addition experiments, using the fast-acting Axl inhibitor R428, suggests a role for virus-induced Axl activation during rLCMV-LASVGP entry but not at later steps of viral replication. Previous studies demonstrated that the HT-1080 cells used in our study induce a robust IFN-I response when challenged with other RNA viruses (82), excluding an overall defect in innate antiviral immunity. The observed difference from flaviviruses may rather be explained by the fact that infection of LCMV and LASV in many cell types, including HT-1080, fails to induce a robust IFN-I response (69, 82–85). The ability of LASV and LCMV to evade innate immunity seems independent of receptor use and is based on the potent IFN antagonist function of the viral NP and Z proteins, which efficiently block IFN-I induction, making attenuation via Axl obsolete (83, 85–88).

Previous studies on Axl-mediated viral entry pinpointed different endocytotic pathways, including macropinocytosis (59) and CME (58), suggesting virus-specific differences. Application of a panel of diagnostic inhibitors revealed that Axl-mediated entry of rLCMV-LASVGP occurs via an endocytotic pathway related to macropinocytosis, as with filoviruses (89) but distinct from Zika virus, which uses CME (58). The Axl-mediated LASV entry pathway uncovered in our present study shares similarities with the recently characterized unusual macropinocytosis-related pathway linked to DG-mediated entry of LASV and LCMV into epithelial cells and fibroblasts (90, 91). However, we also noted important differences. Unlike with DG-mediated viral entry, the pathway linked to Axl depends, e.g., on non-muscle myosin II, required for early macropinosome formation (63), similar to the pathways used by poxviruses (28) and Ebola virus (59). Both DG and Axl mediated internalization and delivery of the virus to endosomes. The similar kinetics of viral endosomal escape suggest convergence of the endocytosis pathways, likely at the level of late endosomes. This is supported by our observation that LASV entry via both receptors critically depends on LAMP-1, making this late endosomal entry factor an attractive target for antiviral therapeutic intervention.

Examination of candidate receptors on endothelial cells revealed coexpression of Axl with an underglycosylated form of DG with relatively low virus-binding affinity. Simultaneous blocking of both DG and Axl was required to affect rLCMV-LASVGP entry, whereas perturbation of the individual candidate receptors had only mild effects, suggesting some degree of redundancy. In line with this observation, viral attachment to endothelial cells was followed by rapid virus-induced tyrosine phosphorylation of both receptors, suggesting that DG and Axl may be engaged during productive viral entry. This seems distinct from the process of Zika virus, which uses Axl as a primary receptor in endothelial cells in a nonredundant manner (76).

In sum, our study confirms and extends previous work supporting the notion that Axl can fulfill different functions in LASV entry in distinct cell types, depending on the extent of the posttranslational modification of DG. Based on the combined information available, we propose the following model for the specific functions of DG and Axl during LASV infection. During zoonotic transmission, highly glycosylated DG present in epithelial cells can rapidly catch and internalize the virus, acting as a primary entry receptor (90). A role for DG glycosylation as a host determinant during virus-human coevolution is indeed suggested by genome-wide association studies that uncovered positive selection for specific LARGE alleles in populations from regions of western African where LASV is endemic (92–94). In severe LASV infection, the virus rapidly spreads via the bloodstream, reaching, among other organs, the liver and the vascular endothelium. In human cells lacking functional DG, the Axl-dependent, DG-independent LASV entry pathway characterized here may be operational. It is, however, unclear whether Axl can function as an authentic entry receptor mediating attachment and internalization or whether its role may be limited to virus attachment, followed by internalization mediated by other, yet-unknown coreceptor(s). Interestingly, chronic infection with hepatitis C virus (HCV) in humans markedly increases Axl expression in the liver (74). Considering the high prevalence of HCV in many regions of western Africa (96), chronic viral hepatitis may contribute to the susceptibility of local populations to LASV infection. Moreover, experimental infection of mice with a hepatotropic isolate of LCMV

resulted in strong upregulation of Axl in liver tissue (95). In endothelial cells, both DG and Axl may contribute to LASV entry, making this cell type highly susceptible and contributing to the endothelial dysfunction that precedes shock and death. Therapeutic strategies against LASV may therefore consider Axl an additional drug target.

MATERIALS AND METHODS

Antibodies and reagents. Monoclonal antibody (MAb) IIH6 anti-α-DG (mouse IgM) was provided by Kevin Campbell (Howard Hughes Medical Institute, University of Iowa). Mouse MAb 8D5 anti-β-DG was purchased from Novocastra. Purified polyclonal goat IgG anti-human Axl, MAb 96201 anti-Dtk/Tyro3, and MAb 120507 anti-DC-SIGN were from R&D Systems. Mouse MAb ab54803 anti-Axl was from Abcam. Mouse MAb sc-20011 anti-LAMP1 was from Santa Cruz Biotechnology. MAb 83.6 to LASV GP2 has been described previously (47), as has MAb 113 anti-LCMV NP (97). MAb cl14a to phospho-β-DG PY982 was from BD Bioscience, and MAb 4G10 to phospho-tyrosine was from St. Cruz Biotechnology. Antibody to the clathrin heavy chain was purchased from BD Biosciences. Other MAbs included mouse MAb B-5-1-2 anti-α-tubulin and goat polyclonal antibody to human IgG Fc (Sigma-Aldrich). Horseradish peroxidase (HRP)-conjugated polyclonal goat anti-mouse IgG, goat anti-mouse IgM, and rabbit anti-goat IgG were from Dako. Fluorescein isothiocyanate (FITC)-conjugated goat anti-mouse IgG was from Jackson ImmunoResearch. The nuclear dye 4′,6-diamidino-2-phenylindole (DAPI) was purchased from Molecular Probes (Eugene, OR). The full-length GPC of Tacaribe virus (TCRV) was kindly provided by Juan-Carlos de la Torre (Scripps Research Institute, La Jolla, CA). The CellTiter-Glo assay system was obtained from Promega (Madison, WI). Annexin V from human placenta conjugated to biotin, heparin, and streptavidin-HRP were from Sigma. The DG fragment DGEKFc4 is comprised of amino acids 1 to 485 of α-DG, followed by an enterokinase (EK) cleavage site and the Fc portion (hinge, CH2, and CH3) of human IgG1 and was produced and purified as described previously (48). For the optimal sensitivity of our assay, DGEKFc4 was produced in cells overexpressing LARGE, resulting in efficient matriglycan modification (14). Inhibitors used in this study included R428 to Axl tyrosine kinase (Sellekchem), Dynasore, Dyngo 4a, pitstop-2 (Ascent Scientific), Pirl1 (Chembridge), CT04, blebbistatin, cytochalasin D, 5-(*N*-ethyl-*N*-isopropyl) amiloride (EIPA), IPA-3, jasplakinolide, latrunculin A, ML-7, ribavirin, and ammonium chloride (NH_4Cl) (Sigma).

Cell culture. Human lung carcinoma alveolar epithelial A549 cells, the human fibrosarcoma cell line HT-1080, HeLa cells, and human embryonic kidney (HEK293H) cells, were cultured in Dulbecco's modified Eagle's medium (DMEM) and 10% (vol/vol) FBS supplemented with glutamine and penicillin-streptomycin. Primary human hepatocytes were isolated from liver specimens obtained after partial hepatectomy at Hannover Medical School and plated at a density of 1.3×10^6 cells on collagen-coated P6 dishes as described previously (35). Cells were kept in hepatocyte culture medium (Lonza) for 1 to 3 days before cell lysis. Cultures were 90% confluent, and cells showed typical hepatocyte morphology with multiple nuclei. Human umbilical vein endothelial cells (HUVEC) (CC-2517), primary human lung microvascular endothelial cells (HMVEC-L) (CC-2527), and primary human small-airway epithelial cells (SAEC) (CC-2547) were purchased from Clonetics/Lonza as cryopreserved specimens and cultured according to the manufacturer's protocol using the endothelial cell growth medium (EGM) BulletKit, the EGM 2MV BulletKit, and small-airway epithelial cell growth medium (CC-3118), respectively. According to the manufacturer's information, HMVEC-L are isolated from small vessels within normal lung tissue cultured to $\geq$90% purity and represent a mixed population of both blood and lymphatic endothelial cells. HUVEC and HMVEC-L were passaged 5 times, which corresponds to $<$15 population doublings, to ensure preservation of the differentiated phenotypes. Expression of the differentiation marker CD31/105 was verified by immunofluorescence staining using MAb 28364 to CD31 (Abcam). SAEC are isolated from normal human lung tissue from the distal portion of the lung in the 1-mm bronchiole area. Cells were passaged 5 times, and differentiation was verified by staining for cytokeratin 19 using MAb ab52625 (Abcam) as recommended by the manufacturer. For infection studies, cells were seeded in collagen- or poly-L-lysine-coated M96 tissue culture plates at 20,000 cells/cm^2, and experiments were performed at a confluence of $>$90% after 2 to 3 days.

Viruses and virus purification. The generation, growth, and titration of recombinant LCMV expressing the envelope GP of LASV strain Josiah (rLCMV-LASVGP) and the G protein of vesicular stomatitis virus (rLCMV-VSVG) have been described elsewhere (39, 98). According to the institutional biosafety guidelines of the Lausanne University Hospital, the chimera rLCMV-LASVGP has been classified as a BSL2 pathogen for use in cell culture. Inactivated LASV strain Josiah was provided by Christina Spiropoulou, Special Pathogens Branch of the Centers for Disease Control and Prevention (Atlanta, GA). Recombinant human adenovirus 5 (AdV-5) expressing GFP has been described previously (99), as has recombinant VSV expressing GFP (100). Recombinant propagation-defective VSV encoding the two reporter proteins GFP and firefly luciferase (Luc) was generated as described previously (101). Recombinant VSV pseudotypes bearing the envelope GP of TCRV were generated as reported earlier (100). To obtain serum-free rLCMV-LASVGP, virus was purified according to a modified protocol of Dutko and Oldstone (102). Briefly, rLCMV-LASVGP was grown in BHK21 cells as described previously (39). Conditioned cell culture supernatants were harvested after 72 h, and virus was precipitated from cleared supernatants by addition of 6.5 g per 100 ml polyethylene glycol 8000 (PEG-8000) with stirring overnight at 6°C. After centrifugation at 8,000 rpm for 30 min at 4°C, the PEG pellet was dissolved in TNE-EGTA (10 mM Tris-HCl, pH 7.5, 100 mM NaCl, 1 mM EDTA, 5 mM EGTA) using 1 ml of TNE-EGTA for 50 ml of the original supernatant. After incubation for 2 h at 4°C, virus was layered on a discontinuous renografin gradient and purified by ultracentrifugation as described previously (102). After dialysis against phosphate-buffered saline (PBS),

infectious virus titers were determined by immunofocus assay on VeroE6 cells in complete medium containing 10% (wt/vol) FBS. Concentrated virus titers were 10^8 to 10^9 PFU/ml. Inactivated LASV obtained as a PEG precipitate from the CDC was treated with TNE-EGTA for 2 h at 4°C, followed by purification over a renografin gradient. A mock preparation was prepared from the conditioned supernatant of uninfected BHK21 cells subjected to PEG precipitation and purification over a renografin gradient, analogously to the virus preparation.

Capture ELISA for rLCMV-LASVGP and inactivated authentic LASV. MAb 83.6 to LASV GP2 (10 μg/ml, 50 μl/well) was added to a 96-well microtiter plate (enzyme immunoassay [EIA]/radioimmunoprecipitation assay [RIA] high-bond plates [Corning]), and immobilization was carried out at room temperature (RT) for 4 h. Wells were washed 3 times with PBS, and nonspecific binding was blocked by adding 200 μl/well 1% (wt/vol) bovine serum albumin (BSA)-PBS for 1 h at RT. For capture of virus, serum-free preparations of rLCMV-LASVGP and inactivated authentic LASV were diluted to 10^7 PFU/ml and added (50 μl/well) in triplicate to immobilized MAb 86.3 for 16 h at 6°C. As a negative control, AdV5-GFP was included. Wells were washed 3 times with PBS. For detection of phosphatidylserine (PS) on bound virus, annexin V (ANX-V) biotin conjugate from human placenta (1:50 in 1% [wt/vol] BSA-PBS) was added overnight at 6°C in the presence and absence of 5 mM EGTA. LASV GP1 was probed with DGEKFc4 (10 μg/ml in 1% [wt/vol] BSA-PBS) overnight at 6°C. Wells were washed 3 times with PBS. Bound ANX-V was detected with streptavidin-HRP at 1:1,000 in 1% (wt/vol) BSA-PBS for 2 h at 6°C and DGEKFc4 with anti-human IgG Fc antibody conjugated to HRP at 1:1,000 in 1% (wt/vol) BSA-PBS for 2 h in the cold. After incubation, the plates were washed four times and developed using 50 μl of 3,3,5,5′-tetramethylbenzidine (eBiosciences, MA). The color reaction was stopped by adding 20 μl of 2 M H_2SO_4. Plates were analyzed using a plate reader spectrophotometer (Tecan, Mannedorf, Switzerland) by measuring the absorbance at 450 nm, with correction at 570 nm. Background binding to wells without immobilized antibody was subtracted, and the ratios of GP1 binding to PS binding were calculated.

Microscale isolation of DG using WGA. Enrichment of DG by wheat germ agglutinin (WGA) affinity purification was carried out by following a modified protocol reported earlier (103). Briefly, two T150 flasks of A549 cells, HT-1080 cells, and HUVEC (>90% confluence) were washed twice with 20 mM HEPES, pH 7.5, 150 mM NaCl. Cells were solubilized in 2 ml of cold solubilization buffer per flask consisting of 50 mM HEPES, pH 7.5, 200 mM NaCl–1% (wt/vol) NP-40, 1.2 mM EDTA, protease inhibitor cocktail complete (Roche), and 1 mM phenylmethylsulfonyl fluoride (PMSF) for 45 min in a cold room. Lysates were cleared by centrifugation for 10 min at 14, 000 rpm in a microcentrifuge, and 5 mM $MgCl_2$ and 10 mM sodium pyrophosphate (final concentration) were added. The WGA matrix (20 μl/ml) was added and incubated on a head-over shaker overnight at 6°C. The WGA matrix was washed 4 times with 10 volumes of 50 mM HEPES, pH 7.5, 200 mM NaCl–0.05% (wt/vol) NP-40, 1.2 mM EDTA, protease inhibitor cocktail, 1 mM PMSF, 5 mM $CaCl_2$, 5 mM $MgCl_2$. Elution of WGA-bound proteins was achieved by incubation of matrix protein four times with 5 volumes of elution buffer (10 mM Tris, pH 8.0, 0.15 M NaCl, 0.2 M *N*-acetylglucosamine) for 15 min at RT. Individual fractions were probed for the presence of DG in a Western blot using MAb 8D5 to β-DG, and the most concentrated factions were pooled, followed by dialysis against PBS.

Solid-phase virus binding assay. The WGA-purified DG fractions derived from A549 cells, HT-1080 cells, and HUVEC (described above) were analyzed by Western blotting, and signals for β-DG were quantified by densitometry to allow immobilization of normalized amounts of DG protein using the dilutions 1:1 for HT-1080, 1:1.32 for HUVEC, and 1:2.02 for A459, carried out overnight at 6°C. Wells were washed 3 times with PBS. Nonspecific binding was blocked by addition of 200 μl/well of 1% (wt/vol) BSA-PBS and incubation for 1 h at RT. Dilutions of rLCMV-LASVGP were prepared in 1% (wt/vol) BSA in PBS, and virus (50 μl/well) was added in triplicate for 16 h at 6°C. Wells were washed 3 times with PBS, and bound virus was detected with MAb 83.6 to LASV GP2 (20 μg/ml) in 1% (wt/vol) BSA in PBS for 16 h at 6°C. After three washes, bound primary antibody was detected using biotinylated goat anti-mouse IgG combined with streptavidin-HRP as described previously (14). Plates were developed as described in the section "Capture ELISA for rLCMV-LASVGP and inactivated authentic LASV" above. Background binding to wells without immobilized DG was subtracted, and binding curves were plotted.

Virus infections. Cells were seeded in 96-well plates at 2×10^4 cells per well and grown in confluent monolayers for 16 to 20 h, unless stated otherwise. Cells were treated with drugs as detailed for the specific experiments, followed by infection with the viruses at the defined multiplicity of infection (MOI) for 1 h at 37°C. Unbound virus was removed, cells were washed twice with DMEM, and fresh medium was added. Infection of rLCMV-LASVGP and rLCMV-VSVG was quantified by detection of LCMV NP in an immunofluorescence assay (IFA) with MAb 113 as described previously (104). VSV pseudotypes, AdV5-GFP, and rVSV-GFP were detected via the GFP reporter using direct fluorescence.

For the determination of the serum dependence of rLCMV-LASVGP infection in HT-1080 cells, serum-free virus was pretreated with complete medium containing increasing concentrations of FBS for 2 h at 4°C. Virus was added to cells for another 2 h at 4°C, followed by washing to remove unbound virus. Cells were shifted to 37°C by adding 200 μl per well of warm complete medium containing 10% (vol/vol) FBS. After 1 h, 20 mM ammonium chloride was added and infection detected after 16 h, as described above.

Blocking with ANX-V was achieved by pretreating serum-free virus with the concentrations of ANX-V in DMEM indicated above with 20 mM HEPES for 2 h at 4°C as described previously (45). The kinetics of endosomal escape was determined as reported previously (90).

For perturbation with antibodies to Axl and DG, M96 plates were chilled on ice, medium was removed, and cells were washed three times with cold serum-free medium containing 2% (wt/vol) BSA and supplemented with 20 mM HEPES. Polyclonal Ab to Axl, MAb IIH6 to DG, and control Ab were diluted

as indicated above in serum-free medium containing 2% (wt/vol) BSA supplemented with 20 mM HEPES and incubated with cells for 2 h at 4°C (50 μl/well). Viruses were prepared at a 10-fold final concentration in medium containing 20% (vol/vol) FBS and supplemented with 20 mM HEPES. Five microliters of a virus inoculum was added to the Ab mixtures on cells, mixed carefully, and incubated for another 2 h at 4°C. Inoculums were removed, cells were washed three times with serum-free medium containing 2% (wt/vol) BSA and supplemented with 20 mM HEPES, and 200 μl/well complete medium was added. Cells were cultured at 37°C and 5% CO_2 for the time periods indicated in the figures and fixed, and infection was assessed as described above.

Flow cytometry analysis. For cell surface staining of HT-1080 cells for Axl and TIM-1, cells were detached with a cell scraper, resuspended in fluorescence-activated cell sorting (FACS) buffer (1% [vol/vol] FCS solution, 0.1% [wt/vol] sodium azide, PBS), and transferred to conical 96-well plates. The primary antibodies polyclonal goat anti-Axl (R&D Biosciences; AF154) and anti-TIM-1 (R&D Biosciences, AF11750) were diluted 1:50 in FACS buffer and incubated on ice for 1 h. Cells were then washed twice in FACS buffer and labeled with the secondary antibody donkey anti-goat IgG conjugated to phycoerythrin (PE) from Jackson ImmunoResearch diluted 1:50 in FACS buffer for 45 min on ice in the dark. After two wash steps in 1% (vol/vol) FBS in PBS, cells were fixed with CellFix solution for 10 min at room temperature in the dark. Cells were washed twice and resuspended in 1% (vol/vol) FBS in PBS. Flow cytometry was performed using a CyAnTM ADP flow cytometer (Beckman Coulter), and data were analyzed with the FlowJo software package (Ashland, OR).

Immunoblotting. For immunoblotting, proteins were separated by SDS-PAGE and transferred to nitrocellulose. After being blocked in 3% (wt/vol) skim milk in PBS, membranes were incubated with 1 to 10 μg/ml primary antibody in 3% (wt/vol) skim milk, PBS overnight at 4°C. After several washes in PBS, 0.1% (wt/vol) Tween 20 (PBST), secondary antibodies coupled to HRP were applied at 1:5,000 in PBST for 1 h at room temperature. In a Western blot detecting tyrosine-phosphorylated Axl and β-DG, membranes were rinsed three times in PBST containing 250 mM NaCl to lower background binding. Membranes were developed by enhanced chemiluminescence (ECL) using a LiteABlot kit (EuroClone). Signals were acquired with an ImageQuant LAS 4000Mini (GE Healthcare Lifesciences) or by exposure to X-ray films. Quantification of Western blots was performed with ImageQuant TL (GE Healthcare Lifesciences).

Generation of DG-deficient HT-1080 cells using lentivirus-delivered shRNA. To deplete DG core protein in HT-1080 cells, a lentiviral vector expressing validated small hairpin RNA (shRNA) targeting human DG (sh-DG) (clone TRCN0000056191, RHS3979-9623375; Thermo Scientific) or a scrambled control shRNA (sh-sc) were generated as described by the ViraPower lentiviral expression system protocol from Invitrogen (United Kingdom). Briefly, a puromycin kill curve determination was performed with HT-1080 cells, with which 2 μg/ml was the minimum puromycin concentration required to kill untransduced cells. For the production of lentiviruses, 3×10^6 HEK293T cells were cultured in 10-cm tissue culture dishes in serum-free 293 SFM II medium (Gibco; catalog no. 11686-029). At 24 h postseeding, fresh medium was added to cells 4 h before the transfection. Calcium chloride (250 mM) and HBS (50 mM HEPES, 1.5 mM Na_2HPO_4, 140 mM NaCl) solutions were used to cotransfect the four required DNA plasmids: pLP1 helper (*gag/pol*), pLP2 helper (*rev*), and pCAGGS/VSVGP with sh-DG 56191 (human pLKO.1) or with the sh-sc (human pLKO.1) shRNA control. Transfected cells were incubated for 16 h at 37°C, medium was replaced with 293 SFM II, and the mixture was incubated for 24 h at 37°C and 5% CO_2. At 40 h posttransfection, cell supernatants were collected and centrifuged for 5 min at 500 $\times$ *g* to remove cellular debris. Each lentivirus was concentrated using the Amicon Ultra-15 centrifugal filter device by ultracentrifugation according to the manufacturer's instructions (Millipore; Ultracel 100KREF, UFC910024). For infection, 5×10^5 HT-1080 cells/well were seeded in 6-well plates and cultured for 24 h at 37°C. The day after, medium was replaced by complete medium supplemented with 6 μg/ml Polybrene and 100 μl of each crude lentivirus stock. The cells were spinoculated at 2,600 rpm for 3 h at 23°C. Cells were then washed twice with medium. Transduced cells were incubated for 72 h at 37°C. After 72 h, cells were washed once with PBS and complete medium supplemented with 2 μg/ml puromycin. After 48 h, cell death was checked and the selective medium replaced every 2 days for 2 weeks. Depletion of DG core protein from HT-1080 cells was verified by Western blotting using MAb 8D5 as described above. DG-deficient cells were passaged a maximum of 10 times, and the DG null phenotype was verified for cells used for our experiments.

RNAi. RNA interference (RNAi) was performed using validated small interfering RNAs (siRNAs) On-Target*plus* SMARTpool for Axl (L-003104-00-0005) and scrambled siRNA (D-001820-10-05) as a control from Thermo Scientific Dharmacon (Lafayette, CO). For the depletion of the clathrin heavy chain, siGenome On-Target*plus* SMARTpool duplex (J-004001-09) to the human clathrin heavy chain and a control siRNA pool were obtained from Dharmacon Research (Lafayette, CO). A pool of the following siRNAs was used: siRNA 1, 5′-GAG AAU GGC UGU ACG UAA U-3′; 2, 5′-UGA GAA AUG UAA UGC GAA U-3′; 3, 5′-GCA GAA GAA UCA ACG UUA U-3′; and 4, 5′-CGU AAG AAG GCU CGA GAG U-3′. Briefly, 3×10^6 HT-1080 cells were reverse transfected with 0.72 μM siRNA in a 10-cm-diameter dish using Lipofectamine RNAiMAX (Invitrogen, Paisley, United Kingdom) according to the manufacturer's recommendation. For LAMP-1 knockdown, 3×10^4 cells/well were seeded overnight in an M96 plate and transfected using Lipofectamine RNAiMAX with All Star scramble RNA or LAMP-1-specific siRNA 5′-CAC GTA ATG CAT TGC CTG TAA-3′ (Qiagen) at a final concentration of 50 nM. At 48 h posttransfection, cells were infected with rLCMV-LASVGP (MOI = 0.1) and rVSVΔG-VSVG (MOI = 0.02) or mock infected. Parallel specimens were lysed to confirm knockdown by Western blotting.

Virus-induced receptor signaling. Purified rLCMV-LASVGP (8.4×10^8 PFU/ml) and equivalent volumes of a mock preparation were incubated in 10 ml HBSS with 10% (vol/vol) FBS for 2 h at 4°C to allow binding of Gas6/PS, followed by layering on a 2-ml cushion of 20% (wt/vol) sucrose in PBS

containing 1 mM $MgCl_2$ and 0.1 mM $CaCl_2$. After being spun at 35,000 rpm for 90 min in an SW41 swing-out rotor, the supernatant was decanted completely. Pellets were resuspended in 250 μl of HBSS for 16 h at 4°C in a closed vial on a shaker. Concentrated virus was titrated by IFA on VeroE6 cells. HT-1080 cells and HMVEC-L were seeded in M6 plates at 4×10^5 cells per well in complete medium and cultured to obtain closed monolayers of >90% confluence. Cells were serum starved for 16 h and chilled on ice for 5 min. Medium was removed, and 4×10^7 PFU of virus was diluted in 1 ml of added serum-free medium, corresponding to an MOI of circa 50. Virus was added to the cells in the cold and incubated for 2 h on ice. To control wells, a mock preparation was added. Cells were washed twice in cold serum-free medium, followed by addition of prewarmed serum-free medium (4 ml/well), and shifted to 37°C. At the time points indicated in the figures, medium was removed and cells were lysed in cold lysis buffer: 1% (wt/vol) NP-40, 50 mM Tris, pH 7.5, 150 mM NaCl, 2 mM EGTA, 0.2 mM EDTA, 50 mM NaF, Complete protease inhibitor cocktail from Roche, and 1 mM PMSF. Cells were scraped off with a plastic cell scraper and passaged 5 times through a blue tip, transferred to a microtube, and incubated on a head-over shaker in a cold room for 30 min. Lysates were cleared by centrifugation at 14,000 rpm in a microcentrifuge for 10 min in the cold. For the detection of tyrosine-phosphorylated β-DG PY892 and β-DG protein with MAbs cl14a and 8D5, respectively, total protein was extracted (105) and separated by SDS-PAGE, and Western blotting was performed as described above. For the detection of the tyrosine phosphorylation of Axl, total Axl was isolated by immunoprecipitation (IP) using a modified protocol reported by Meertens et al. (58). For this purpose, purified polyclonal goat anti-IgG was immobilized on cyanogen bromide-activated Sepharose 4B (Sigma) by following the manufacturer's recommendations. Anti-Axl matrix was mixed with cleared lysate (10 μl of matrix per ml of lysate) and incubated on a head-over shaker for 4 h or overnight in a cold room. After IP overnight, the matrix was washed four times with lysis buffer and once with lysis buffer without detergent. Immunocomplexes were eluted by boiling the mixtures in reducing SDS-PAGE sample buffer for 5 min, followed by separation by SDS-PAGE using Tris-glycine running gels with 5.5% (wt/vol) polyacrylamide to achieve optimal separation of Axl from the IgG heavy chain. Axl protein was revealed in a Western blot using an anti-Axl mouse MAb, and tyrosine phosphorylation was detected in anti-Axl IP using an MAb to tyrosine phosphate.

ACKNOWLEDGMENTS

We thank Gert Zimmer, Division of Virology, Institute of Virology and Immunology, Mittelhäusern, Switzerland, for the vesicular stomatitis virus pseudotype system. Inactivated LASV Josiah was provided by Christina Spiropoulou from the Special Pathogens Branch of the Centers for Disease Control and Prevention, Atlanta, GA, USA. Antibody IIH6 to α-DG was a gift from Kevin Campbell, Howard Hughes Medical Institute, University of Iowa, Iowa City, IA. We further thank Antonella Pasquato and Sylvia Rothenberger for helpful discussions.

This research was supported by Swiss National Science Foundation grants 310030_149746 and 310030_170108 to S.K. and funds to S.K. from the University of Lausanne, as well as grants from the Human Frontier Science Program (LT-000048-2009) and the German Research Foundation (DFG, GE 2145/3-1) to G.G.

REFERENCES

1. McCormick JB, Fisher-Hoch SP. 2002. Lassa fever. Curr Top Microbiol Immunol 262:75–109.
2. Geisbert TW, Jahrling PB. 2004. Exotic emerging viral diseases: progress and challenges. Nat Med 10:S110–S121. https://doi.org/10.1038/nm1142.
3. Sweileh WM. 2017. Global research trends of World Health Organization's top eight emerging pathogens. Global Health 13:9. https://doi.org/10.1186/s12992-017-0233-9.
4. Fisher-Hoch SP, Tomori O, Nasidi A, Perez-Oronoz GI, Fakile Y, Hutwagner L, McCormick JB. 1995. Review of cases of nosocomial Lassa fever in Nigeria: the high price of poor medical practice. BMJ 311:857–859. https://doi.org/10.1136/bmj.311.7009.857.
5. Stephenson EH, Larson EW, Dominik JW. 1984. Effect of environmental factors on aerosol-induced Lassa virus infection. J Med Virol 14:295–303. https://doi.org/10.1002/jmv.1890140402.
6. Borio L, Inglesby T, Peters CJ, Schmaljohn AL, Hughes JM, Jahrling PB, Ksiazek T, Johnson KM, Meyerhoff A, O'Toole T, Ascher MS, Bartlett J, Breman JG, Eitzen EM, Jr, Hamburg M, Hauer J, Henderson DA, Johnson RT, Kwik G, Layton M, Lillibridge S, Nabel GJ, Osterholm MT, Perl TM, Russell P, Tonat K. 2002. Hemorrhagic fever viruses as biological weapons: medical and public health management. JAMA 287:2391–2405. https://doi.org/10.1001/jama.287.18.2391.
7. Yun NE, Walker DH. 2012. Pathogenesis of Lassa fever. Viruses 4:2031–2048. https://doi.org/10.3390/v4102031.
8. McCormick JB, King IJ, Webb PA, Johnson KM, O'Sullivan R, Smith ES, Trippel S, Tong TC. 1987. A case-control study of the clinical diagnosis and course of Lassa fever. J Infect Dis 155:445–455. https://doi.org/10.1093/infdis/155.3.445.
9. McCormick JB, King IJ, Webb PA, Scribner CL, Craven RB, Johnson KM, Elliott LH, Belmont-Williams R. 1986. Lassa fever. Effective therapy with ribavirin. N Engl J Med 314:20–26.
10. Buchmeier MJ, de la Torre JC, Peters CJ. 2007. Arenaviridae: the viruses and their replication, p 1791–1828. *In* Knipe DL, Howley PM (ed), Fields virology, 4th ed. Lippincott-Raven, Philadelphia, PA.
11. Cao W, Henry MD, Borrow P, Yamada H, Elder JH, Ravkov EV, Nichol ST, Compans RW, Campbell KP, Oldstone MB. 1998. Identification of alpha-dystroglycan as a receptor for lymphocytic choriomeningitis virus and Lassa fever virus. Science 282:2079–2081. https://doi.org/10.1126/science.282.5396.2079.
12. Barresi R, Campbell KP. 2006. Dystroglycan: from biosynthesis to pathogenesis of human disease. J Cell Sci 119:199–207. https://doi.org/10.1242/jcs.02814.
13. Yoshida-Moriguchi T, Campbell KP. 2015. Matriglycan: a novel polysaccharide that links dystroglycan to the basement membrane. Glycobiology 25:702–713. https://doi.org/10.1093/glycob/cwv021.
14. Kunz S, Rojek JM, Kanagawa M, Spiropoulou CF, Barresi R, Campbell KP, Oldstone MB. 2005. Posttranslational modification of alpha-

dystroglycan, the cellular receptor for arenaviruses, by the glycosyltransferase LARGE is critical for virus binding. J Virol 79:14282–14296. https://doi.org/10.1128/JVI.79.22.14282-14296.2005.
15. Rojek JM, Spiropoulou CF, Campbell KP, Kunz S. 2007. Old World and clade C New World arenaviruses mimic the molecular mechanism of receptor recognition used by alpha-dystroglycan's host-derived ligands. J Virol 81:5685–5695. https://doi.org/10.1128/JVI.02574-06.
16. Inamori K, Yoshida-Moriguchi T, Hara Y, Anderson ME, Yu L, Campbell KP. 2012. Dystroglycan function requires xylosyl- and glucuronyltransferase activities of LARGE. Science 335:93–96. https://doi.org/10.1126/science.1214115.
17. Praissman JL, Willer T, Sheikh MO, Toi A, Chitayat D, Lin YY, Lee H, Stalnaker SH, Wang S, Prabhakar PK, Nelson SF, Stemple DL, Moore SA, Moremen KW, Campbell KP, Wells L. 2016. The functional O-mannose glycan on alpha-dystroglycan contains a phospho-ribitol primed for matriglycan addition. Elife 5:e14473. https://doi.org/10.7554/eLife.14473.
18. Goddeeris MM, Wu B, Venzke D, Yoshida-Moriguchi T, Saito F, Matsumura K, Moore SA, Campbell KP. 2013. LARGE glycans on dystroglycan function as a tunable matrix scaffold to prevent dystrophy. Nature 503:136–140. https://doi.org/10.1038/nature12605.
19. Briggs DC, Yoshida-Moriguchi T, Zheng T, Venzke D, Anderson ME, Strazzulli A, Moracci M, Yu L, Hohenester E, Campbell KP. 2016. Structural basis of laminin binding to the LARGE glycans on dystroglycan. Nat Chem Biol 12:810–814. https://doi.org/10.1038/nchembio.2146.
20. Jae LT, Raaben M, Riemersma M, van Beusekom E, Blomen VA, Velds A, Kerkhoven RM, Carette JE, Topaloglu H, Meinecke P, Wessels MW, Lefeber DJ, Whelan SP, van Bokhoven H, Brummelkamp TR. 2013. Deciphering the glycosylome of dystroglycanopathies using haploid screens for Lassa virus entry. Science 340:479–483. https://doi.org/10.1126/science.1233675.
21. Hastie KM, Zandonatti MA, Kleinfelter LM, Heinrich ML, Rowland MM, Chandran K, Branco LM, Robinson JE, Garry RF, Saphire EO. 2017. Structural basis for antibody-mediated neutralization of Lassa virus. Science 356:923–928. https://doi.org/10.1126/science.aam7260.
22. Walker DH, McCormick JB, Johnson KM, Webb PA, Komba-Kono G, Elliott LH, Gardner JJ. 1982. Pathologic and virologic study of fatal Lassa fever in man. Am J Pathol 107:349–356.
23. Dylla DE, Xie L, Michele DE, Kunz S, McCray PB, Jr. 2011. Altering alpha-dystroglycan receptor affinity of LCMV pseudotyped lentivirus yields unique cell and tissue tropism. Genet Vaccines Ther 9:8. https://doi.org/10.1186/1479-0556-9-8.
24. Shimojima M, Stroher U, Ebihara H, Feldmann H, Kawaoka Y. 2012. Identification of cell surface molecules involved in dystroglycan-independent Lassa virus cell entry. J Virol 86:2067–2078. https://doi.org/10.1128/JVI.06451-11.
25. Goncalves AR, Moraz ML, Pasquato A, Helenius A, Lozach PY, Kunz S. 2013. Role of DC-SIGN in Lassa virus entry into human dendritic cells. J Virol 87:11504–11515. https://doi.org/10.1128/JVI.01893-13.
26. Lemke G, Burstyn-Cohen T. 2010. TAM receptors and the clearance of apoptotic cells. Ann N Y Acad Sci 1209:23–29. https://doi.org/10.1111/j.1749-6632.2010.05744.x.
27. Lemke G, Rothlin CV. 2008. Immunobiology of the TAM receptors. Nat Rev Immunol 8:327–336. https://doi.org/10.1038/nri2303.
28. Mercer J, Helenius A. 2008. Vaccinia virus uses macropinocytosis and apoptotic mimicry to enter host cells. Science 320:531–535. https://doi.org/10.1126/science.1155164.
29. Amara A, Mercer J. 2015. Viral apoptotic mimicry. Nat Rev Microbiol 13:461–469. https://doi.org/10.1038/nrmicro3469.
30. Moller-Tank S, Maury W. 2014. Phosphatidylserine receptors: enhancers of enveloped virus entry and infection. Virology 468-470:565–580. https://doi.org/10.1016/j.virol.2014.09.009.
31. Jemielity S, Wang JJ, Chan YK, Ahmed AA, Li W, Monahan S, Bu X, Farzan M, Freeman GJ, Umetsu DT, Dekruyff RH, Choe H. 2013. TIM-family proteins promote infection of multiple enveloped viruses through virion-associated phosphatidylserine. PLoS Pathog 9:e1003232. https://doi.org/10.1371/journal.ppat.1003232.
32. Durbeej M, Henry MD, Ferletta M, Campbell KP, Ekblom P. 1998. Distribution of dystroglycan in normal adult mouse tissues. J Histochem Cytochem 46:449–457. https://doi.org/10.1177/002215549804600404.
33. Peyrard M, Seroussi E, Sandberg-Nordqvist AC, Xie YG, Han FY, Fransson I, Collins J, Dunham I, Kost-Alimova M, Imreh S, Dumanski JP. 1999. The human LARGE gene from 22q12.3-q13.1 is a new, distinct member of the glycosyltransferase gene family. Proc Natl Acad Sci U S A 96:598–603. https://doi.org/10.1073/pnas.96.2.598.
34. de Bernabe DB, Inamori K, Yoshida-Moriguchi T, Weydert CJ, Harper HA, Willer T, Henry MD, Campbell KP. 2009. Loss of alpha-dystroglycan laminin binding in epithelium-derived cancers is caused by silencing of LARGE. J Biol Chem 284:11279–11284. https://doi.org/10.1074/jbc.C900007200.
35. Kleine M, Riemer M, Krech T, DeTemple D, Jager MD, Lehner F, Manns MP, Klempnauer J, Borlak J, Bektas H, Vondran FW. 2014. Explanted diseased livers—a possible source of metabolic competent primary human hepatocytes. PLoS One 9:e101386. https://doi.org/10.1371/journal.pone.0101386.
36. Kanagawa M, Saito F, Kunz S, Yoshida-Moriguchi T, Barresi R, Kobayashi YM, Muschler J, Dumanski JP, Michele DE, Oldstone MB, Campbell KP. 2004. Molecular recognition by LARGE is essential for expression of functional dystroglycan. Cell 117:953–964. https://doi.org/10.1016/j.cell.2004.06.003.
37. Durbeej M, Campbell KP. 1999. Biochemical characterization of the epithelial dystroglycan complex. J Biol Chem 274:26609–26616. https://doi.org/10.1074/jbc.274.37.26609.
38. Barresi R, Michele DE, Kanagawa M, Harper HA, Dovicio SA, Satz JS, Moore SA, Zhang W, Schachter H, Dumanski JP, Cohn RD, Nishino I, Campbell KP. 2004. LARGE can functionally bypass alpha-dystroglycan glycosylation defects in distinct congenital muscular dystrophy. Nat Med 10:696–703. https://doi.org/10.1038/nm1059.
39. Rojek JM, Sanchez AB, Nguyen NT, de la Torre JC, Kunz S. 2008. Different mechanisms of cell entry by human-pathogenic Old World and New World arenaviruses. J Virol 82:7677–7687. https://doi.org/10.1128/JVI.00560-08.
40. Pasqual G, Rojek JM, Masin M, Chatton JY, Kunz S. 2011. Old world arenaviruses enter the host cell via the multivesicular body and depend on the endosomal sorting complex required for transport. PLoS Pathog 7:e1002232. https://doi.org/10.1371/journal.ppat.1002232.
41. Moraz ML, Pythoud C, Turk R, Rothenberger S, Pasquato A, Campbell KP, Kunz S. 2013. Cell entry of Lassa virus induces tyrosine phosphorylation of dystroglycan. Cell Microbiol 15:689–700. https://doi.org/10.1111/cmi.12078.
42. Rojek JM, Moraz ML, Pythoud C, Rothenberger S, Van der Goot FG, Campbell KP, Kunz S. 2012. Binding of Lassa virus perturbs extracellular matrix-induced signal transduction via dystroglycan. Cell Microbiol 14:1122–1134. https://doi.org/10.1111/j.1462-5822.2012.01784.x.
43. Lee AM, Cruite J, Welch MJ, Sullivan B, Oldstone MB. 2013. Pathogenesis of Lassa fever virus infection: I. Susceptibility of mice to recombinant Lassa Gp/LCMV chimeric virus. Virology 442:114–121. https://doi.org/10.1016/j.virol.2013.04.010.
44. Sommerstein R, Ramos da Palma J, Olschlager S, Bergthaler A, Barba L, Lee BP, Pasquato A, Flatz L. 2014. Evolution of recombinant lymphocytic choriomeningitis virus/Lassa virus in vivo highlights the importance of the GPC cytosolic tail in viral fitness. J Virol 88:8340–8348. https://doi.org/10.1128/JVI.00236-14.
45. Morizono K, Xie Y, Olafsen T, Lee B, Dasgupta A, Wu AM, Chen IS. 2011. The soluble serum protein Gas6 bridges virion envelope phosphatidylserine to the TAM receptor tyrosine kinase Axl to mediate viral entry. Cell Host Microbe 9:286–298. https://doi.org/10.1016/j.chom.2011.03.012.
46. Fernandez-Fernandez L, Bellido-Martin L, Garcia de Frutos P. 2008. Growth arrest-specific gene 6 (GAS6). An outline of its role in haemostasis and inflammation. Thromb Haemost 100:604–610.
47. Weber EL, Buchmeier MJ. 1988. Fine mapping of a peptide sequence containing an antigenic site conserved among arenaviruses. Virology 164:30–38. https://doi.org/10.1016/0042-6822(88)90616-2.
48. Kunz S, Calder L, Oldstone MB. 2004. Electron microscopy of an alpha-dystroglycan fragment containing receptor sites for lymphocytic choriomeningitis virus and laminin, and use of the receptoid body as a reagent to neutralize virus. Virology 325:207–215. https://doi.org/10.1016/j.virol.2004.04.044.
49. Kondratowicz AS, Lennemann NJ, Sinn PL, Davey RA, Hunt CL, Moller-Tank S, Meyerholz DK, Rennert P, Mullins RF, Brindley M, Sandersfeld LM, Quinn K, Weller M, McCray PB, Jr, Chiorini J, Maury W. 2011. T-cell immunoglobulin and mucin domain 1 (TIM-1) is a receptor for Zaire Ebolavirus and Lake Victoria Marburgvirus. Proc Natl Acad Sci U S A 108:8426–8431. https://doi.org/10.1073/pnas.1019030108.
50. Ohkuma S, Poole B. 1978. Fluorescence probe measurement of the intralysosomal pH in living cells and the perturbation of pH by various agents. Proc Natl Acad Sci U S A 75:3327–3331. https://doi.org/10.1073/pnas.75.7.3327.
51. Ohkuma S, Poole B. 1981. Cytoplasmic vacuolation of mouse peritoneal

macrophages and the uptake into lysosomes of weakly basic substances. J Cell Biol 90:656–664. https://doi.org/10.1083/jcb.90.3.656.
52. Jae LT, Raaben M, Herbert AS, Kuehne AI, Wirchnianski AS, Soh TK, Stubbs SH, Janssen H, Damme M, Saftig P, Whelan SP, Dye JM, Brummelkamp TR. 2014. Virus entry. Lassa virus entry requires a trigger-induced receptor switch. Science 344:1506–1510. https://doi.org/10.1126/science.1252480.
53. Mercer J, Schelhaas M, Helenius A. 2010. Virus entry by endocytosis. Annu Rev Biochem 79:803–833. https://doi.org/10.1146/annurev-biochem-060208-104626.
54. Marsh M, Helenius A. 2006. Virus entry: open sesame. Cell 124:729–740. https://doi.org/10.1016/j.cell.2006.02.007.
55. Grove J, Marsh M. 2011. The cell biology of receptor-mediated virus entry. J Cell Biol 195:1071–1082. https://doi.org/10.1083/jcb.201108131.
56. Myers SH, Brunton VG, Unciti-Broceta A. 2016. AXL inhibitors in cancer: a medicinal chemistry perspective. J Med Chem 59:3593–3608. https://doi.org/10.1021/acs.jmedchem.5b01273.
57. Holland SJ, Pan A, Franci C, Hu Y, Chang B, Li W, Duan M, Torneros A, Yu J, Heckrodt TJ, Zhang J, Ding P, Apatira A, Chua J, Brandt R, Pine P, Goff D, Singh R, Payan DG, Hitoshi Y. 2010. R428, a selective small molecule inhibitor of Axl kinase, blocks tumor spread and prolongs survival in models of metastatic breast cancer. Cancer Res 70:1544–1554. https://doi.org/10.1158/0008-5472.CAN-09-2997.
58. Meertens L, Labeau A, Dejarnac O, Cipriani S, Sinigaglia L, Bonnet-Madin L, Le Charpentier T, Hafirassou ML, Zamborlini A, Cao-Lormeau VM, Coulpier M, Misse D, Jouvenet N, Tabibiazar R, Gressens P, Schwartz O, Amara A. 2017. Axl mediates ZIKA virus entry in human glial cells and modulates innate immune responses. Cell Rep 18:324–333. https://doi.org/10.1016/j.celrep.2016.12.045.
59. Hunt CL, Kolokoltsov AA, Davey RA, Maury W. 2011. The Tyro3 receptor kinase Axl enhances macropinocytosis of Zaire ebolavirus. J Virol 85:334–347. https://doi.org/10.1128/JVI.01278-09.
60. Mercer J, Helenius A. 2009. Virus entry by macropinocytosis. Nat Cell Biol 11:510–520. https://doi.org/10.1038/ncb0509-510.
61. Krzyzaniak MA, Zumstein MT, Gerez JA, Picotti P, Helenius A. 2013. Host cell entry of respiratory syncytial virus involves macropinocytosis followed by proteolytic activation of the F protein. PLoS Pathog 9:e1003309. https://doi.org/10.1371/journal.ppat.1003309.
62. Johannsdottir HK, Mancini R, Kartenbeck J, Amato L, Helenius A. 2009. Host cell factors and functions involved in vesicular stomatitis virus entry. J Virol 83:440–453. https://doi.org/10.1128/JVI.01864-08.
63. Mercer J, Helenius A. 2012. Gulping rather than sipping: macropinocytosis as a way of virus entry. Curr Opin Microbiol 15:490–499. https://doi.org/10.1016/j.mib.2012.05.016.
64. Koivusalo M, Welch C, Hayashi H, Scott CC, Kim M, Alexander T, Touret N, Hahn KM, Grinstein S. 2010. Amiloride inhibits macropinocytosis by lowering submembranous pH and preventing Rac1 and Cdc42 signaling. J Cell Biol 188:547–563. https://doi.org/10.1083/jcb.200908086.
65. Cohen-Dvashi H, Cohen N, Israeli H, Diskin R. 2015. Molecular mechanism for LAMP1 recognition by Lassa virus. J Virol 89:7584–7592. https://doi.org/10.1128/JVI.00651-15.
66. Cohen-Dvashi H, Israeli H, Shani O, Katz A, Diskin R. 2016. Role of LAMP1 binding and pH sensing by the spike complex of Lassa virus. J Virol 90:10329–10338. https://doi.org/10.1128/JVI.01624-16.
67. Israeli H, Cohen-Dvashi H, Shulman A, Shimon A, Diskin R. 2017. Mapping of the Lassa virus LAMP1 binding site reveals unique determinants not shared by other Old World arenaviruses. PLoS Pathog 13:e1006337. https://doi.org/10.1371/journal.ppat.1006337.
68. Fisher-Hoch S, McCormick JB, Sasso D, Craven RB. 1988. Hematologic dysfunction in Lassa fever. J Med Virol 26:127–135. https://doi.org/10.1002/jmv.1890260204.
69. Lukashevich IS, Maryankova R, Vladyko AS, Nashkevich N, Koleda S, Djavani M, Horejsh D, Voitenok NN, Salvato MS. 1999. Lassa and Mopeia virus replication in human monocytes/macrophages and in endothelial cells: different effects on IL-8 and TNF-alpha gene expression. J Med Virol 59:552–560. https://doi.org/10.1002/(SICI)1096-9071(199912)59:4<552::AID-JMV21>3.0.CO;2-A.
70. Sotgia F, Bonuccelli G, Bedford M, Brancaccio A, Mayer U, Wilson MT, Campos-Gonzalez R, Brooks JW, Sudol M, Lisanti MP. 2003. Localization of phospho-beta-dystroglycan (pY892) to an intracellular vesicular compartment in cultured cells and skeletal muscle fibers in vivo. Biochemistry 42:7110–7123. https://doi.org/10.1021/bi0271289.
71. Yamauchi Y, Helenius A. 2013. Virus entry at a glance. J Cell Sci 126:1289–1295. https://doi.org/10.1242/jcs.119685.
72. Torriani G, Galan-Navarro C, Kunz S. 2017. Lassa virus cell entry reveals new aspects of virus-host cell interaction. J Virol 91:e01902-16. https://doi.org/10.1128/JVI.01902-16.
73. Gay CM, Balaji K, Byers LA. 2017. Giving AXL the axe: targeting AXL in human malignancy. Br J Cancer 116:415–423. https://doi.org/10.1038/bjc.2016.428.
74. Read SA, Tay ES, Shahidi M, O'Connor KS, Booth DR, George J, Douglas MW. 2015. Hepatitis C virus driven AXL expression suppresses the hepatic type I interferon response. PLoS One 10:e0136227. https://doi.org/10.1371/journal.pone.0136227.
75. Schlie K, Maisa A, Freiberg F, Groseth A, Strecker T, Garten W. 2010. Viral protein determinants of Lassa virus entry and release from polarized epithelial cells. J Virol 84:3178–3188. https://doi.org/10.1128/JVI.02240-09.
76. Liu S, DeLalio LJ, Isakson BE, Wang TT. 2016. AXL-mediated productive infection of human endothelial cells by Zika virus. Circ Res 119:1183–1189. https://doi.org/10.1161/CIRCRESAHA.116.309866.
77. Meertens L, Carnec X, Lecoin MP, Ramdasi R, Guivel-Benhassine F, Lew E, Lemke G, Schwartz O, Amara A. 2012. The TIM and TAM families of phosphatidylserine receptors mediate dengue virus entry. Cell Host Microbe 12:544–557. https://doi.org/10.1016/j.chom.2012.08.009.
78. Bhattacharyya S, Zagorska A, Lew ED, Shrestha B, Rothlin CV, Naughton J, Diamond MS, Lemke G, Young JA. 2013. Enveloped viruses disable innate immune responses in dendritic cells by direct activation of TAM receptors. Cell Host Microbe 14:136–147. https://doi.org/10.1016/j.chom.2013.07.005.
79. Brindley MA, Hunt CL, Kondratowicz AS, Bowman J, Sinn PL, McCray PB, Jr, Quinn K, Weller ML, Chiorini JA, Maury W. 2011. Tyrosine kinase receptor Axl enhances entry of Zaire ebolavirus without direct interactions with the viral glycoprotein. Virology 415:83–94. https://doi.org/10.1016/j.virol.2011.04.002.
80. Rothlin CV, Ghosh S, Zuniga EI, Oldstone MB, Lemke G. 2007. TAM receptors are pleiotropic inhibitors of the innate immune response. Cell 131:1124–1136. https://doi.org/10.1016/j.cell.2007.10.034.
81. Rothlin CV, Lemke G. 2010. TAM receptor signaling and autoimmune disease. Curr Opin Immunol 22:740–746. https://doi.org/10.1016/j.coi.2010.10.001.
82. Pythoud C, Rothenberger S, Martinez-Sobrido L, de la Torre JC, Kunz S. 2015. Lymphocytic choriomeningitis virus differentially affects the virus-induced type I interferon response and mitochondrial apoptosis mediated by RIG-I/MAVS. J Virol 89:6240–6250. https://doi.org/10.1128/JVI.00610-15.
83. Martinez-Sobrido L, Zuniga EI, Rosario D, Garcia-Sastre A, de la Torre JC. 2006. Inhibition of the type I interferon response by the nucleoprotein of the prototypic arenavirus lymphocytic choriomeningitis virus. J Virol 80:9192–9199. https://doi.org/10.1128/JVI.00555-06.
84. Martinez-Sobrido L, Giannakas P, Cubitt B, Garcia-Sastre A, de la Torre JC. 2007. Differential inhibition of type I interferon induction by arenavirus nucleoproteins. J Virol 81:12696–12703. https://doi.org/10.1128/JVI.00882-07.
85. Xing J, Ly H, Liang Y. 2014. The Z proteins of pathogenic but not non-pathogenic arenaviruses inhibit the RIG-I-like receptor-dependent interferon production. J Virol 89:2944–2955. https://doi.org/10.1128/JVI.03349-14.
86. Martinez-Sobrido L, Emonet S, Giannakas P, Cubitt B, Garcia-Sastre A, de la Torre JC. 2009. Identification of amino acid residues critical for the anti-interferon activity of the nucleoprotein of the prototypic arenavirus lymphocytic choriomeningitis virus. J Virol 83:11330–11340. https://doi.org/10.1128/JVI.00763-09.
87. Qi X, Lan S, Wang W, Schelde LM, Dong H, Wallat GD, Ly H, Liang Y, Dong C. 2010. Cap binding and immune evasion revealed by Lassa nucleoprotein structure. Nature 468:779–783. https://doi.org/10.1038/nature09605.
88. Russier M, Pannetier D, Baize S. 2012. Immune responses and Lassa virus infection. Viruses 4:2766–2785. https://doi.org/10.3390/v4112766.
89. Hunt CL, Lennemann NJ, Maury W. 2012. Filovirus entry: a novelty in the viral fusion world. Viruses 4:258–275. https://doi.org/10.3390/v4020258.
90. Oppliger J, Torriani G, Herrador A, Kunz S. 2016. Lassa virus cell entry via dystroglycan involves an unusual pathway of macropinocytosis. J Virol 90:6412–6429. https://doi.org/10.1128/JVI.00257-16.
91. Iwasaki M, Ngo N, de la Torre JC. 2014. Sodium hydrogen exchangers contribute to arenavirus cell entry. J Virol 88:643–654. https://doi.org/10.1128/JVI.02110-13.
92. Sabeti PC, Varilly P, Fry B, Lohmueller J, Hostetter E, Cotsapas C, Xie X,

Byrne EH, McCarroll SA, Gaudet R, Schaffner SF, Lander ES, Frazer KA, Ballinger DG, Cox DR, Hinds DA, Stuve LL, Gibbs RA, Belmont JW, Boudreau A, Hardenbol P, Leal SM, Pasternak S, Wheeler DA, Willis TD, Yu F, Yang H, Zeng C, Gao Y, Hu H, Hu W, Li C, Lin W, Liu S, Pan H, Tang X, Wang J, Wang W, Yu J, Zhang B, Zhang Q, Zhao H, Zhou J, Gabriel SB, Barry R, Blumenstiel B, Camargo A, Defelice M, Faggart M, Goyette M, et al. 2007. Genome-wide detection and characterization of positive selection in human populations. Nature 449:913–918. https://doi.org/10.1038/nature06250.

93. Andersen KG, Shylakhter I, Tabrizi S, Grossman SR, Happi CT, Sabeti PC. 2012. Genome-wide scans provide evidence for positive selection of genes implicated in Lassa fever. Philos Trans R Soc Lond B Biol Sci 367:868–877. https://doi.org/10.1098/rstb.2011.0299.
94. Andersen KG, Shapiro BJ, Matranga CB, Sealfon R, Lin AE, Moses LM, Folarin OA, Goba A, Odia I, Ehiane PE, Momoh M, England EM, Winnicki S, Branco LM, Gire SK, Phelan E, Tariyal R, Tewhey R, Omoniwa O, Fullah M, Fonnie R, Fonnie M, Kanneh L, Jalloh S, Gbakie M, Saffa S, Karbo K, Gladden AD, Qu J, Stremlau M, Nekoui M, Finucane HK, Tabrizi S, Vitti JJ, Birren B, Fitzgerald M, McCowan C, Ireland A, Berlin AM, Bochicchio J, Tazon-Vega B, Lennon NJ, Ryan EM, Bjornson Z, Milner DA, Jr, Lukens AK, Broodie N, Rowland M, Heinrich M, Akdag M, et al. 2015. Clinical sequencing uncovers origins and evolution of Lassa virus. Cell 162:738–750. https://doi.org/10.1016/j.cell.2015.07.020.
95. Beier JI, Jokinen JD, Holz GE, Whang PS, Martin AM, Warner NL, Arteel GE, Lukashevich IS. 2015. Novel mechanism of arenavirus-induced liver pathology. PLoS One 10:e0122839. https://doi.org/10.1371/journal.pone.0122839.
96. Mora N, Adams WH, Kliethermes S, Dugas L, Balasubramanian N, Sandhu J, Nde H, Small C, Jose J, Scaglione S, Layden JE. 2016. A synthesis of hepatitis C prevalence estimates in Sub-Saharan Africa: 2000–2013. BMC Infect Dis 16:283. https://doi.org/10.1186/s12879-016-1584-1.
97. Buchmeier MJ, Lewicki HA, Tomori O, Oldstone MB. 1981. Monoclonal antibodies to lymphocytic choriomeningitis and pichinde viruses: generation, characterization, and cross-reactivity with other arenaviruses. Virology 113:73–85. https://doi.org/10.1016/0042-6822(81)90137-9.
98. Pinschewer DD, Perez M, Sanchez AB, de la Torre JC. 2003. Recombinant lymphocytic choriomeningitis virus expressing vesicular stomatitis virus glycoprotein. Proc Natl Acad Sci U S A 100:7895–7900. https://doi.org/10.1073/pnas.1332709100.
99. Kunz S, Sevilla N, McGavern DB, Campbell KP, Oldstone MB. 2001. Molecular analysis of the interaction of LCMV with its cellular receptor α-dystroglycan. J Cell Biol 155:301–310. https://doi.org/10.1083/jcb.200104103.
100. Kunz S, Rojek JM, Perez M, Spiropoulou CF, Oldstone MB. 2005. Characterization of the interaction of Lassa fever virus with its cellular receptor alpha-dystroglycan. J Virol 79:5979–5987. https://doi.org/10.1128/JVI.79.10.5979-5987.2005.
101. Berger Rentsch M, Zimmer G. 2011. A vesicular stomatitis virus replicon-based bioassay for the rapid and sensitive determination of multi-species type I interferon. PLoS One 6:e25858. https://doi.org/10.1371/journal.pone.0025858.
102. Dutko FJ, Oldstone MB. 1983. Genomic and biological variation among commonly used lymphocytic choriomeningitis virus strains. J Gen Virol 64(Part 8):1689–1698. https://doi.org/10.1099/0022-1317-64-8-1689.
103. Michele DE, Barresi R, Kanagawa M, Saito F, Cohn RD, Satz JS, Dollar J, Nishino I, Kelley RI, Somer H, Straub V, Mathews KD, Moore SA, Campbell KP. 2002. Post-translational disruption of dystroglycan-ligand interactions in congenital muscular dystrophies. Nature 418:417–422. https://doi.org/10.1038/nature00837.
104. Kunz S, Sevilla N, Rojek JM, Oldstone MB. 2004. Use of alternative receptors different than alpha-dystroglycan by selected isolates of lymphocytic choriomeningitis virus. Virology 325:432–445. https://doi.org/10.1016/j.virol.2004.05.009.
105. Wessel D, Flugge UI. 1984. A method for the quantitative recovery of protein in dilute solution in the presence of detergents and lipids. Anal Biochem 138:141–143. https://doi.org/10.1016/0003-2697(84)90782-6.